Mitochondrial Import of Malat1 Regulates Cardiac Mitochondrial Function in Type 2 Diabetes Mellitus through Interaction with MicroRNA-23b

Quincy A. Hathaway
West Virginia University School of Medicine https://orcid.org/0000-0001-8226-2319
Andrew D. Taylor
West Virginia University School of Medicine
Amina Kunovac
West Virginia University School of Medicine
Mark V. Pinti
West Virginia University School of Medicine
Mackenzie S. Newman
West Virginia University School of Medicine
Chris C. Cook
West Virginia University School of Medicine
Michael T. Winters
West Virginia University School of Medicine
Emily Westemeier
West Virginia University School of Medicine
Garrett K. Fink
West Virginia University School of Medicine
Andrya J. Durr
West Virginia University School of Medicine
Danielle L. Shepherd
West Virginia University School of Medicine
Aaron R. Robart
West Virginia University School of Medicine
Ivan Martinez
West Virginia University School of Medicine
John M. Hollander (jhollander@hsc.wvu.edu)
West Virginia University School of Medicine https://orcid.org/0000-0001-5724-694X

Original investigation

Keywords: Bioinformatics, Heart, Long Non-Coding RNA, Machine Learning

Posted Date: December 16th, 2020

DOI: https://doi.org/10.21203/rs.3.rs-127504/v1

Abstract

Background: The pathogenesis of type 2 diabetes mellitus is known to alter cardiac mitochondrial bioenergetics, but the role of non-coding RNAs (ncRNAs) in regulating this process remains poorly understood, specifically within the mitochondrion. Here we characterized the mitochondrial localization of nuclear-encoded lncRNAs in the heart in an effort to understand how import of lncRNAs can modify mitochondrial function during diabetes mellitus.

Methods: Human patient and FVB/NJ mouse cardiac tissues were collected from type 2 diabetics and non-diabetics. Immunoblotting was used to validate purity of mitochondrial fractionation. NcRNA from subcellular compartments (cytoplasmic and mitochondrial) were sequenced through the Illumina 2500 HiSeq. LncRNA mitochondrial targeting sequences were acquired through crosslinking immunoprecipitation (CLIP) with Polynucleotide Phosphorylase (PNPase) and secondary structures were analyzed using supervised and unsupervised machine learning algorithms. Fluorescence in situ hybridization (FISH) allowed for visualization of Malat1 localization. Mitochondrial function was assessed through oxygen consumption rate.

Results: 2448 LncRNAs were discovered in human cardiac mitochondria. Malat1 and microRNA-23b abundance were significantly reduced in human and mouse diabetic mitochondria. Modification of the import protein PNPase in HL-1 cells decreased binding affinity (~80%) of transcript variant 4 of Malat1 (Malat1-204), with machine learning (AUC 0.75) identifying stem-loops as shared secondary structures of lncRNAs bound to PNPase. Knockdown of Malat1-204 and microRNA-23b in mitochondria decreased protein expression of mt-Nd4 (~55%), though showed little/no binding homology to the mt-Nd4 mRNA transcript. Malat1-204 and microRNA-23b were identified bound to mt-Rnr1 rRNA, which could influence translation of mt-Nd4 through the mitochondrial 12S rRNA pathway.

Conclusions: Malat1-204 and microRNA-23b, decreased in cardiac diabetic mitochondria, likely stabilize the mitochondrial ribosomal complexes through binding of mt-Rnr1. The significant decrease in total abundance of lncRNAs in diabetic mitochondria could suggest maladaptation for regulating bioenergetics and managing future insults.

Background

Long non-coding RNAs (lncRNAs) are a class of regulatory RNAs that assume multiple responsibilities within the cell. These lncRNAs have previously been demonstrated to be involved in both nuclear and cytoplasmic cellular processes such as: regulating chromatin structure, histone modifications, mRNA transcription, microRNA (miRNA) sponging, and regulation of protein translation and modification [1, 2]. Though the roles played by lncRNAs in the cytoplasm are an area of current exploration, their function in other subcellular regions remains largely unexplored. The mitochondrion represents an isolated, spatially-dense region within the cell that may provide a unique environment that stoichiometrically favors interactions between lncRNAs and other RNA species. Recent investigations have assessed the

involvement of lncRNA in altering mitochondrial function [3], but the direct interactions of lncRNA, and other ncRNA, within the mitochondrion remain largely unknown.

The mitochondrial genome is comprised of 2 rRNAs, 22 tRNAs, and 13 coding mRNAs [4]. Work from our group, and others, has demonstrated that miRNAs imported into mitochondria regulate the mitochondrial genome through inhibition [5–7] or activation [8] of mitochondrial-encoded genes. Additionally, the production of miRNAs [9] and lncRNAs [10, 11] from the mitochondrial genome itself have been shown to contribute to the overall mitochondrial ncRNA regulatory network. Only recently has the concept of nuclear-encoded lncRNA localization into the mitochondrion been explored [12, 13], challenging our understanding of the import mechanisms required to facilitate this process and the extent of lncRNAs being sequestered. As a greater number of nuclear-encoded ncRNAs are found within the mitochondrion, a framework for interpreting the overall role of specific ncRNAs in regulating mitochondrial and cellular health is needed.

Studies to date have mainly focused on a limited number of imported miRNAs and their effects on mitochondrial transcription and health. While these efforts have been informative, the global aspects of miRNA diversity remain largely unexplored. Expression profiles within the mitochondrion reveal large quantities of miRNAs [5, 14–16], even in the absence of mitochondrial DNA [17]. While ongoing research is continuing to expand our understanding of ncRNA regulation of the mitochondrial genome, it begs the question: why would a large ncRNA regulatory network be required for maintaining 13 mitochondrial transcribed genes? Imported miRNAs have been reported to alter expression of the mitochondrial genome, but a large portion of miRNAs show little, or no, homology with mitochondrially-derived sequences [5, 16]. In understanding the abundance of ncRNAs within the mitochondrion, import/export pathways may provide details regarding the criteria necessary for a ncRNA to become included in a mitochondrial regulatory network.

Polynucleotide phosphorylase (PNPase) is a ribonuclease that is conserved across bacterial, archaeal, and eukaryotic domains of life [18, 19]. In bacteria, PNPase is a primary regulator of mRNA degradation [20], modifying the cellular response to temperature change [21] and biofilm formation [22], as well as functioning as a processing enzyme for long RNA [23]. Progressing through the evolutionary timeline, eukaryotic PNPase is localized specifically to the intermembrane space of the mitochondrion, seemingly lacking its previously defined functional roles. In 2010, Wang et al. first established an RNA import function for PNPase in mammalian systems [24], revealing that tRNA and ribozyme machinery are transported by PNPase into the mitochondrion. Additionally, changes in PNPase expression have resulted in alterations in cellular function and miRNA import [6, 25]. PNPase, through its KH and S1 RNA binding domains, may provide a functional context for ncRNA import and regulation in the mitochondrion.

In the current study, we investigated the ncRNA network in cardiac mitochondria and its changes in type 2 diabetes mellitus. Through comparison of both cytoplasmic and isolated mitochondrial ncRNA populations, we identified hundreds of nuclear-encoded ncRNAs in the mitochondrion, including the lncRNAs MALAT1, NEAT1, and KCNQ1OT1 whose abundance were significantly decreased as a result of

type 2 diabetes mellitus. Specifically, we examined the mechanisms controlling localization of Malat1 to mitochondria and the regulatory role the lncRNA plays on mitochondrial function. Transcript variant 4 of Malat1 (Malat1-204) was shown to bind to PNPase, which may act as a shuttle for import of lncRNA mediated by recognition of specific RNA secondary structures. Malat1-204, through stabilization of mitochondrial mRNA transcripts such as mt-Nd4, may influence changes in protein expression during diabetic insult. With the present data, we suggest that the mitochondrion has a dynamic ncRNA network that can be modified by type 2 diabetes mellitus in the heart.

Results

Mitochondrial Isolation

To evaluate the subcellular localization of non-coding RNA (ncRNA), assessments of fractionation purity were performed. Tissue homogenization, differential centrifugation, and sucrose gradient separation allowed for the enrichment of pure populations of cardiac mitochondria (Fig. 1A). Mitochondrial contamination was determined through the presence of cytoplasmic ribosomal RNA (rRNA) 18S and 28S within mitochondrial RNA fractions (Fig. 1B). While a loss of 18S and 28S rRNA is typically considered a measure of RNA degradation, proper isolation of mitochondrial RNA retains minimal traces of cytoplasmic rRNA and will therefore have a low RNA integrity number (RIN) [5, 14].

Immunoblotting further confirmed purification of mitochondrial fractions, indicated by an absence of nuclear (HDAC6) and cytoplasmic proteins (GAPDH), with inclusion of mitochondrial proteins (COX IV) (Fig. 1C). The presence of COX IV in cytoplasmic fractions is likely due to nuclear-encoded mitochondrial proteins, such as COX IV, being transported to the mitochondrion following translation in the cytoplasm [26]. Additionally, HDAC6 is found both in the nucleus and cytoplasm [27], indicated by its appearance in the in the isolated cytoplasm (Fig. 1C). QPCR of two randomly chosen mitochondrially-derived mRNA revealed a significant difference (~ 40–50 fold) between mitochondrial and cytoplasmic compartments (Fig. 1D). Sequencing data indicated a reduced expression of mitochondrial transcribed genes within the cytoplasm compared to mitochondria by up to 1,100-fold (Additional File 1). Mitochondrial populations revealed a clear separation from cytoplasmic portions of the cell.

Mitochondrial Long non-coding RNA (lncRNA) Profiles

While miRNAs have been identified in the mitochondrion, we wanted to assess whether other nuclear-encoded ncRNA species were present in the mitochondrion, and if these profiles were altered during type 2 diabetic insult. Using a long non-coding RNA (lncRNA) sequencing approach on sucrose-purified mitochondria, we identified a variety of ncRNAs which were differentially compartmentalized in both the type 2 diabetic human (top) and DbDb mouse (bottom) heart (Fig. 2A). Of the lncRNAs identified in the mitochondrion, MALAT1 was the most differentially compartmentalized in both human and mouse mitochondrial sequencing results, defined as the lncRNA with the lowest adjusted *P* value (P_{adj}) (Fig. 2B). The presented PCA plots in Fig. 2C illustrate the dispersion between cytoplasmic and mitochondrial ncRNA samples in both human (top) and mouse (bottom). Comparing the dispersion observed in the

mitochondrial groups, the human diabetic and non-diabetic groups showed a more prominent between group variation than the mouse cohort (Fig. 2C, Figure S2A and B). Differential expression profiles for all ncRNA genes in human and mouse (mitochondrial and cytoplasmic) cohorts are provided (Additional File 1). LncRNAs, as well as other ncRNAs, were present in the mitochondria with type 2 diabetic insult significantly altering expression profiles.

Cytoplasmic and Mitochondrial Stratification Resulting from Type 2 Diabetes Mellitus

To understand how the ncRNA expression profiles are altered between the subcellular compartments (cytoplasm and mitochondria) and disease states (diabetic and non-diabetic), we assessed the number of differentially compartmentalized genes for each combination in human (left) and mouse (right) (Fig. 3A). Using these comparisons, we tracked the fold change (presented as the Log_2 change) to quantitate the abundance of ncRNAs in each group. In type 2 diabetic compared to non-diabetic mitochondria, the majority of differentially compartmentalized genes were significantly downregulated (Fig. 3B, top right panel). Additionally, large variations in differentially expressed ncRNAs existed between the cytoplasmic and mitochondrial compartments (Fig. 3B, bottom panels). Of the lncRNAs differentially compartmentalized, MALAT1 and NEAT1 abundance were both significantly decreased in both the human and mouse analyses (Additional File 1). To validate these findings, qPCR for Malat1 transcript variant 4 (Malat1-204) and Neat1 transcript variant 2 (Neat1-202) were performed in a separate population of mitochondria isolated from mouse cardiac tissue (Fig. 3C). To further highlight the differences across the subcellular compartments and disease states, heatmaps displaying the top 500 genes with the lowest P_{adj} value are displayed (Fig. 3D) for human (top) and mouse (bottom), with differences indicated as the fold change deviation from the mean of the data. The mitochondrial fractions of ncRNAs have distinct profiles in both pathogenic and non-pathogenic states, with diabetic mitochondrial fractions losing lncRNA abundance, such as MALAT1 when compared to controls. Fewer changes are observed in the cytoplasmic fraction of ncRNAs between disease states.

LncRNA-mRNA-miRNA Networks in the Mitochondrion

The mitochondrial interactome, previously understood as miRNAs and mitochondrially transcribed mRNA, is significantly expanded by the presence of lncRNA. Small RNA sequencing was performed in human atrial appendages to determine the distribution of miRNAs in the diabetic and non-diabetic state (Fig. 4A), the complete list of differentially compartmentalized genes provided (Additional File 1). The top fifty most abundant miRNAs and lncRNAs in the human patient samples, as determined by the baseMean value of counts for each gene, are displayed as circles in respect to total number of counts (size), Log_2 fold change (color), and if the gene is differentially expressed (green text) (Fig. 4B). MiRNA1-2 and TTN-AS1 were the most abundant miRNA and lncRNA in the human datasets, respectively. To gain insight into the interactive network of lncRNA-mRNA-miRNA, differentially compartmentalized genes in both the miRNA (human) and lncRNA (human and mouse) datasets were plotted with the thirteen mitochondrially transcribed electron transport chain mRNAs (Fig. 4C). Interactions were determined by experimentally

validated RNA-RNA binding regions characterized on the NPInter (v4.0) server and highlight the binding affinities that exist between each mitochondrially transcribed mRNA and ncRNAs found in the mitochondrion. The circles are determined by the total number of counts (size) and Log_2 fold change (color) (Fig. 4C).

Modeling interactions, as described in Fig. 4B and C, provide only potential binding information and which target biomolecules may be involved. Cross linking immunoprecipitation (CLIP) can act as a mechanistic framework for mapping precise regions of RNAs that may be interacting in a functional context. Using purified mitochondria from mouse cardiac tissue, we performed CLIP analysis for Ago2, Fxr1, and PNPase, revealing the unique distributions of each of these binding proteins (Fig. 4D) and how their binding varies across multiple classes of RNA (Figure S2C). The distribution of CLIP sequencing mappings to each of the ncRNA classes is provided (Figure S3A and B). The Venn diagram (Fig. 4E) illustrates how genes identified through CLIP are differentially regulated depending on the protein assayed; CLIP with Ago2 and Fxr1, both components of the RNA-induced silencing complex (RISC), show more commonalties than compared with PNPase. Of the differentially regulated genes, Ago2 and Fxr1 CLIP associated genes were primarily upregulated when compared to PNPase CLIP associated genes (Fig. 4F, Figure S3C). CLIP of Ago2 and Fxr1 showed higher binding affinities for miRNAs, with PNPase predominately binding lncRNAs (Additional File 1).

Malat1 Distribution and Interactions with Polynucleotide Phosphorylase (PNPase)

Having demonstrated that MALAT1 and other lncRNAs specifically localize within the mitochondrion; we next explored potential proteins that mediate this specific lncRNA compartmentalization process. Fluorescent *in situ* hybridization (FISH) revealed that Malat1, while predominately present in the nucleus, can be identified in the cytoplasm (Fig. 5A, Figure S4A). Further, coupling FISH with MitoTracker™ staining suggested that a co-localization of Malat1 with mitochondria also occurred (Figure S4B), similar to recent findings in hepatocellular carcinoma cells [13]. This indicates that Malat1, whether fragmented or as a native transcript, has the capacity to reach the mitochondrion where it can interact with the organelle.

PNPase may be involved in shuttling Malat1, and other lncRNAs, through its KH and S1 RNA binding domains. Using an HL-1 immortalized mouse cardiomyocyte cell line, we transfected cells with overexpression vectors (Fig. 5B). Overexpression of constructs was demonstrated through immunoblotting, with a shift in size between the full length, KH domain knockout, and S1 domain knockout (Fig. 5C). Using CLIP for PNPase in each of the cell variants, RNA was purified from each of the overexpression groups through SDS-PAGE gel electrophoresis, with a representative gel illustrated (Fig. 5D). Examination of the RNA bound to PNPase, revealed that Malat1-204 expression was significantly downregulated when the S1 domain was removed from PNPase (Fig. 5E), suggesting its role in RNA-protein interactions. Functionally, basal respiration and ATP production were significantly decreased in both the KH and S1 domain knockout groups, with maximal respiration and proton leak

decreased in the S1 domain knockout group (Fig. 5F). These results suggest that PNPase has binding affinity for Malat1, most likely through the KH and/or S1 RNA binding domains.

Mitochondrial RNA Targeting and Structure Analyses

CLIP is a technique that takes advantage of UV crosslinking to examine short RNA regions bound to a protein of interest, leading to both the identification of the RNA bound and the specific region(s) involved in binding [28]. Examining the CLIP PNPase sequencing data, we wanted to determine if a mitochondrial RNA targeting sequence or secondary structure exists that would predict the binding of lncRNA to PNPase and act as a mechanism for lncRNA import. A 60 nt region, directly centered on reads acquired from sequencing, was implemented to determine RNA primary sequence and secondary structure homology through RNAfold [29]. RNAfold secondary structures for human MALAT1, NEAT1, and KCNQ1OT1 illustrate that RNA sequences bound to PNPase are found in stem-loop structures in both the full length (Figure S5) and 60 nt isolated regions (Figure S6A). This includes the Malat1-204 transcript identified in mice (Figure S5). Previous literature has demonstrated the advantages of using machine learning in the classification of lncRNA [30, 31]. We applied a similar supervised machine learning approach to determine if we could predict the primary sequence or secondary structure of the lncRNA responsible for binding to PNPase. Implementing 10-fold cross validation for Support Vector Machines (SVM) and Classification and Regression Trees (CART), machine learning was applied to 50 human and 50 mouse lncRNA 60 nt reads found to bind to PNPase (positives) and 100 randomly generated 60 nt sequences (negatives) [32] (Table S2). Both SVM and CART attained close to 75% prediction accuracy on the entire dataset, for classification of either positive or negative 60 nt sequences (Figure S6B and Table S2).

Assessing sensitivity and specificity, prediction of the lncRNA fragments compared to the random sequence controls revealed an area under the curve (AUC) of ~ 0.75 (Figure S6C); this suggests that the sequences, or RNA secondary structures, possess distinct properties needed to bind PNPase and are identifiable through machine learning. To determine the degree of heterogeneity between the lncRNA regions bound to PNPase, unsupervised learning through CART was applied to examine separation into four subtypes (Figure S6D). 10-fold cross validation was further applied to each of the subtypes compared to the 100 negative sequences, (Table S2), revealing the distinct primary and secondary structure differences between sequences identified to bind to PNPase (Figure S6E). Further, parameters of the LncFinder algorithms that examined base-pairing probability (acguD (Figure S7A) and acgu-ACGU (Figure S7B)) suggested that RNA bound to PNPase has a greater propensity for unpaired loop structures, with differences also in the folding energy (Figure S7C) and sequence GC content (Figure S7D). Both supervised (Additional File 1) and unsupervised CART models suggest that secondary structure, not primary sequence, is important for RNA identification by the mitochondrion.

Malat1-204 Regulation of Mitochondrial Translation

To understand the biological function of Malat1 in the mitochondrion, we wanted to assess potential mechanisms of action. We visualized the mapped sequence reads from the mouse CLIP data for Ago2 and Fxr1 (Fig. 6A), to show the distribution of coverage across the mitochondrial genome. RNA

sequencing in mitochondria revealed significantly decreased mRNA expression of mitochondrially encoded NADH:ubiquinone oxidoreductase core subunit 2 (mt-Nd2) and mitochondrially encoded NADH:ubiquinone oxidoreductase core subunit 4 (mt-Nd4) in type 2 diabetic patients (Figure S7E), with no changes in mitochondrial mRNA expression in the mouse model (Additional File 1). Revealing little perturbation to mitochondrial transcription in the disease, we wanted to understand if ncRNAs played a more significant role in post-transcriptional regulation of mitochondrial mRNA. *In vitro*, we examined a lncRNA (Malat1-204) and miRNA (miRNA-23b-3p) that were decreased in patients with diabetes mellitus as well as crosslinked with Ago2 and Fxr1 in mitochondria. Malat1-204 and miRNA-23b-3p were knocked down in an HL-1 cell line and revealed decreased expression of mt-Nd4 (Fig. 6B), but not mt-Nd2 (Fig. 6C), in both knockdown groups. Further, we characterized the functional consequences of the knockdown *in vitro*, revealing a decreased maximal respiration in Malat1-204 knockdown cells (Fig. 6D).

To understand how Malat1-204 and miRNA-23b-3p could regulate mitochondrial transcription and/or translation, we used IntaRNA 2.0 (Fig. 6E) to predict binding sites across the mitochondrial transcriptome and found that Malat1-204 and miRNA-23b-3p both have binding sites on mitochondrially encoded 12S rRNA (mt-Rnr1) and mt-Nd4. The Ago2 and Fxr1 CLIPs confirmed that the predicted binding sites of Malat1-204 and miRNA-23b-3p aligned to validated clusters of reads on the mt-Rnr1 transcript (Fig. 6F), while the mt-Nd4 predicted binding sites showed little to no association with CLIP data (Figure S7F). Further, the specific complementary regions of Malat1-204 and miRNA-23b-3p predicted to bind mt-Rnr1 were also found in the CLIP datasets (Fig. 6G). No DNA-RNA binding sites were found along the mitochondrial genome, demonstrated by implementing RGT-TDF in human and mouse for MALAT1 (data not shown). Binding of Malat1-204 and/or miRNA-23b-3p to mt-Rnr1 could stabilize the mitochondrial translational machinery, regulating translational efficiency of mtDNA-encoded mRNA transcripts.

Mitochondrial Malat1 Functional Pathway

Our hypothesized mitochondrial lncRNA import pathway and interaction network is illustrated in Fig. 7. As an example, the stem-loop region of Malat1 can bind to the KH and S1 RNA binding domains of PNPase, facilitating its transport across the inner mitochondrial membrane. Within the mitochondrion, lncRNA could serve diverse functions, one of which could be the interaction of Malat1 with the 12S rRNA to regulate translation of mtDNA-encoded mRNA transcripts. Additionally, Ago2 and Fxr1 may help facilitate the contact of Malat1, as well as miRNAs such as miRNA-23b-3p, with the ribosomal complex. Depletion of lncRNAs in the diabetic state, such as Malat1, could highlight the loss of control of mitochondrial function/bioenergetics.

Discussion

In this study we fully characterize the mitochondrial ncRNA network in the heart, which helps to expand our understanding of the presence and purpose of ncRNAs in cardiac mitochondria and how disease states, such as diabetes mellitus, can alter this network. Our data indicate that decreased compartmentalization of lncRNAs in the mitochondrion, such as Malat1, leads to alterations in the expression and processing of mitochondrial mRNA. We suggest that a unique transcript variant of Malat1

(Malat1-204) is imported via the intermembrane space protein PNPase and modifies the translational capacity of the mitochondrial ribosomes through interactions with mt-Rnr1. Malat1, as well as other compartmentalized lncRNAs, exist as part of the mitochondrial regulatory axis, which may play a pivotal role in both the sequestration of other ncRNAs and the maintenance of mitochondrial function during diabetes mellitus.

Kren et al. was one of the first to postulate the idea of sequestration [15]. In a microarray study discovering 15 miRNAs, the authors suggested that due to miRNAs inhibiting multiple mRNA targets, those mRNA may be shuttled into the mitochondria and regulated during specific cellular conditions. While the field has generally moved away from this idea of sequestration, there may be significant biological advantages to operating under these conditions. Our data supports the concept that sequestration may be aided by the enrichment of RNA species in the specific compartment of mitochondria, leading to alterations of transcriptional/translational regulatory networks in four ways. 1) The number of miRNAs, lncRNAs, and other ncRNAs found within and/or directly interacting with the mitochondrion is likely greater than 1,000 different species. The mitochondrial genome, composed of 13 transcribed genes, lacks an inherent diversity for targeting by all of the ncRNAs [33]. 2) The stoichiometric ratio of some RNAs, specifically lncRNA and miRNA, could be significantly elevated in a sub-compartment of the cell [34, 35]. LncRNA, which may exist in the cytoplasm at a relatively low abundance, can be amplified through localization into the mitochondrion. 3) MALAT1, NEAT1, and many of the other lncRNAs found in the sequencing data have experimentally verified RNA-RNA interaction regions with nuclear-encoded miRNAs in the mitochondria [36]. 4) The mitochondrial matrix provides an environment promoting lncRNA folding/processing. High concentrations of magnesium and manganese ions may promote the stabilization of lncRNA secondary and tertiary structures [37–39], along with further processing through small nuclear RNA (snoRNA) [40] **(Additional File 1)**.

While sequestration is an attractive hypothesis for the role of ncRNAs in the mitochondrion, to-date, most investigations have focused on their direct mediation of mitochondrial function [3, 12]. This has come predominantly in the form of miRNA inhibition of mitochondrial mRNA transcription or translation, with few studies detailing the role of ncRNAs as positive influencers of gene expression. The studies that suggest a positive influence of ncRNAs in the mitochondrion appeal to higher-order functions of ncRNAs on mitochondrial transcription/translation, rather than a simple miRNA to mRNA targeting paradigm. An *in silico* assessment of primary non function in the liver suggests a role of miRNAs to bind directly to the mitochondrial DNA and altering transcription, potentiating effects across multiple transcripts [41]. Aside from the regulation of the mitochondrial DNA, Zhang et al. proposed the concept of mediation of translation through regulation of the mitochondrial ribosome [8]. This concept, which is further validated in the current study, suggests that Ago2 can act as an intermediary between ncRNA and the 12S rRNA.

The presence of Ago2 in the mitochondrion has been documented in a number of studies [5, 6, 8, 14, 42]. Ago2, a member of the RNA-induced silencing complex (RISC), acts in a coordinated fashion with miRNA or other small RNA fragments to translocate to complementary regions of RNA. Both the current study and Zhang et al. [8] show that Ago2 not only localizes to the mitochondrion, but can complementarily

bind to rRNA, specifically 12S. Additionally, the RISC-associated protein fragile X mental retardation syndrome-related protein 1 (Fxr1) is shown to have a similar binding capacity, suggesting co-localization. The implications and mechanisms of Ago2 binding to mitochondrial rRNA are still uncertain, but the data presented in this study suggest that Malat1, and potentially miRNAs such as miRNA-23b-3p, can regulate translation through 12S binding. While we only demonstrate that protein expression of mt-Nd4 is decreased following Malat1 knockdown, it is likely that Malat1 influences the expression of the other mitochondrial-derived mRNAs through the same mechanism. Malat1 may have many functional contexts within the mitochondrion, but little is known regarding its mitochondrial import.

While not directly accessible to the cytoplasm or mitochondrial matrix, studies have reported the ability of PNPase to interact with and transport RNAs into the mitochondrion [24, 43]. The KH and S1 RNA binding domains of PNPase are suggested as the mechanism for channeling ncRNA through the mitochondrial intermembrane space into the matrix [24]. Importantly, Wang et al. suggested that a stem-loop sequence on the RNA was necessary for mitochondrial import [24]. These findings support a mechanism whereby PNPase recognition requires RNA secondary structure as opposed to sequence specificity, which is consistent with our findings, including the PNPase CLIP sequencing and machine learning approaches. The framework from LncFinder and the machine learning algorithms begins to provide an archetype for designing personalized lncRNA sequences to target to the mitochondrion; specifically, through incorporating stem-loop structures with more unpaired bases within the loop structures. The proposed strategy for designing mitochondrial imported ncRNAs could be implemented as a novel therapeutic intervention for diabetes mellitus and other diseases with dysregulated ncRNA profiles to restore, remove, and/or introduce new ncRNA into the mitochondrion.

Conclusion

The shared features of lncRNA bound to PNPase highlight a novel mitochondrial RNA import mechanism, through the existence of stem-loop secondary structures, and are suggestive of a pathway to enter the mitochondrion. Within the mitochondrion, lncRNA have the capacity to interact with other ncRNAs, altering the expression of the mitochondrial genome. Malat1-204 has the capacity to both bind mitochondrial transcribed mRNA as well as regulate the translational process of the mitochondrial ribosomal complex through its 12S rRNA. The mitochondrial ncRNA network proposed in this study provides a new perspective on cardiac mitochondrial biology by expanding our concepts of mitochondrial complexity, introducing ncRNA mediators for functional pathways such as bioenergetics, and promoting new therapeutic approaches in the heart when addressing type 2 diabetic disease progression.

Materials And Methods

Study Approval and Patient Population

The West Virginia University Institutional Review Board and Institutional Biosafety Committee approved the studies and data generated from this work (IRB#: 1812394926), including all tissue and patient

information acquired [44]. Informed consent was obtained from all patients by the Heart and Vascular Institute, J.W. Ruby Memorial Hospital at West Virginia University School of Medicine. Right atrial appendages were removed during open-heart and/or valvular surgeries and all tissue and data were stored in a double de-identified process. There was no incentive provided for patients. Surgeries were performed on both type 2 diabetic and non-diabetic patients, following consultation with the surgical team. Non-diabetic patients (HbA1c < 6.5 with no previous diagnosis of diabetes mellitus) and type 2 diabetic patients (HbA1c > 6.5 or with a previous diagnosis of diabetes mellitus) were designated in the study. Patients' tissue was used irrespective of sex, race, or ethnicity. Patients enrolled in the study were not part of a clinical trial. The design and execution of the study was supported by the National Heart, Lung, and Blood Institute [R01 HL-128485]. All procedures performed in studies involving human participants were in accordance with the ethical standards of the institutional and/or national research committee and with the 1964 Helsinki Declaration and its later amendments or comparable ethical standards.

Murine Model

The West Virginia University Animal Care and Use Committee approved all animal studies, including animal housing, sedation, euthanasia, and experimentation. These studies conformed to the most current National Institutes of Health (NIH) Guidelines for the Care and Use of Laboratory Animals manual. FVB/NJ (wild type) and FVB/NJ *Lepr*$^{db+/+-}$ (DbDb) male and female mice were housed in the West Virginia University Health Sciences Center Animal Facility and given access to a rodent diet and water *ad libitum*. FVB/NJ *Lepr*$^{db+/-}$ heterozygous mice were bred together to obtain a homozygous (FVB/NJ *Lepr*$^{db+/+}$) diabetic model. We have previously reported on the cardiovascular deficits of this model [6, 45, 46]. Animals in the wild-type and diabetic groups were aged to 25 weeks and were euthanized. Euthanasia was performed by sedating mice with 5% isoflurane through nose cone administration and subsequently implementing cervical dislocation. Both sexes were evaluated indiscriminately.

Mitochondrial Isolations

Mitochondria were isolated from both human right atrial tissue and mouse whole heart. Differential centrifugation allowed for the compartmentalization of nuclear, cytoplasmic, and mitochondrial fractions. Mitochondrial subpopulations, subsarcolemmal and interfibrillar, were combined to form a total mitochondrial population. Mitochondria were further purified through use of a sucrose gradient (23%, 15%, 10% and 3% percoll solution), as previously described [5].

PNPase Overexpression Constructs

Express Cloning Vectors were synthesized through GenScript (Piscataway, NJ) using the pcDNA3.1 + N-eGFP backbone. Sequences for the full length PNPase protein (FL), KH domain knockout of exon 23 of PNPase (KH), and the S1 domain knockout of the C-terminus of PNPase (S1) were cloned into vectors and the complete sequence information is provided (Figure S1). Vectors were then transfected into a bacterial cell line (DH5α), grown through antibiotic selection, and plasmid DNA was isolated for transfection.

Immortalized HL-1 murine cardiomyocytes were cultured at 37^{o}C, 5% CO_2, as previously described [5, 6, 47]. Briefly, cells were divided into five groups; no plasmid control (NP), pcDNA3.1 + N-eGFP only (GFP), FL, KH, and S1. In the GFP, FL, KH, and S1 sets, 10 µg of each respective plasmid was transfected. Media, with the Lipofectamine 3000, remained on the cells for 48 hours followed by cell imaging using the EVOS™ FL Auto Imaging System (Thermo Fisher) on the GFP fluorescent and phase contrast channels. Cells were washed with PBS, dissociated with 0.05% Trypsin, and preserved at -80^{o}C.

Malat1 and mmu-MiRNA-23b-3p Knockdown

Briefly, cells were divided into four groups; no siRNA control, scramble control, miRNA-23b knockdown (KD), and Malat1 KD. 30 nM of siRNA or scramble was used for transfections. Media, with the Lipofectamine 3000, remained on the cells for 72 hours followed by cell detachment.

Malat1 Fluorescent In Situ Hybridization (FISH)

HL-1 cells were seeded on 18 mm round #1 coverslips in 6-well dishes and were allowed to reach 70–80% confluency, with growth conditions provided above. Cells were incubated with 250 nM of MitoTracker™ Deep Red FM (Thermo Fisher) in Opti-MEM™ (Thermo Fisher) growth media for 30 minutes, and then washed with Claycomb media. The cells were incubated with the Stellaris® RNA FISH Hybridization Buffer containing either a Malat1 or Gapdh probe for 16 hours at 37^{o}C in darkness. Cells were imaged using the Nikon A1R/SIM (Nikon, Minato City, Tokyo, Japan) confocal microscope. Images were processed using the NIS Elements AR (Nikon) software.

Mitochondrial Bioenergetics

The HL-1 cells treated with either the PNPase overexpression constructs or siRNA were plated on a Seahorse XF96 V3 cell culture microplate at a density of 45,000 cells, determined by the Countess II FL Automated Cell Counter (Thermo Fisher). Cells were incubated overnight and the following day analyzed with a Seahorse XF Cell Mito Stress Test Kit (Agilent Technologies, Santa Clara, CA) on the Seahorse XF96 Analyzer (Agilent Technologies), per manufacturer's instructions. Information regarding how the assay was performed has been previously described [48].

Crosslinking Immunoprecipitation (CLIP)

Cells in the NP, GFP, FL, KH, and S1 groups were re-suspended in PBS and transferred to a 24-well plate on ice. Crosslinking was performed using the CX-2000 Crosslinker (Analytik Jena, Upland, CA) at (400 mJ/cm^2) 5 times, as previously described [5]. CLIP was also performed on isolated mitochondria from cardiac tissue of human and mouse diabetic and non-diabetic samples. The protocol was performed as described above, but with slight modifications. In place of incubation with anti-GFP, samples were incubated with either anti-PNPase (human) or anti-Ago2, anti-Fxr1, or anti-PNPase (mouse). All washes, treatments, and extraction of RNA were performed as described above.

Western Blotting

Using 4–12% gradient gels, immunoblotting was performed through MOPS SDS-PAGE, as previously described [48–50]. Densitometry was analyzed using ImageJ and Fiji Software (NIH, Bethesda, MD). For CLIP samples, the area of nitrocellulose membrane containing the GFP (cells) or Ago2, Fxr1, and PNPase (human/mouse) fluorescent region was excised and saved for RNA analysis.

RNA Isolation/Quantitative PCR

Using the miRNeasy Mini Kit (product no.: 217004, Qiagen, Hilden, Germany), per manufacturer's instructions, RNA was isolated from 20 mg of human right atrial tissue and mouse whole heart, as well as from samples of nitrocellulose membrane containing RNA derived from CLIP samples. All primer sequences are provided (Table S1) and primers were designed through NCBI Primer BLAST and Primer3 [51].

Long non-coding RNA (LncRNA) Sequencing

RNA, isolated from human atrial appendages and mouse whole heart (as described above), was sequenced through the West Virginia University Genomics Core Facility. The complete differential expression profiles of mitochondrial and cytoplasmic groups are included (Additional File 1).

Small ncRNA Sequencing

RNA isolated from human atrial appendages and mouse whole heart (as described above) was sequenced through the West Virginia University Genomics Core Facility. The complete differential expression profiles are included (Additional File 1).

High-Throughput Sequencing Crosslinking Immunoprecipitation (HITS-CLIP)

CLIP RNA (as described above) from human atrial appendages (anti-PNPase) and mouse whole heart (anti-Ago2, anit-Fxr1, and anti-PNPase) was sequenced through the West Virginia University Genomics Core Facility. The complete differential expression profiles, along with the raw counts values for each sample are included (Additional File 1).

Statistics

A two-sided Student's t-test or one-way analysis of variance (ANOVA) were used to determine statistical differences, where appropriate. Multiple groups were assessed through Tukey's multiple comparisons test following the ANOVA. Differences between groups were considered statistically significant if $P \leq 0.05$, denoted by *. Data are presented as the mean ± standard error of the mean (SEM), when appropriate. For all sequencing data, raw counts > 1 were considered in statistical analyses. The false-discovery rate (FDR) was set to 0.05 and all significance was determined through a P adjusted value (P_{adj}) < 0.05 using Wald testing.

Declarations

Ethics approval and consent to participate

Human Participants

The West Virginia University Institutional Review Board and Institutional Biosafety Committee approved the studies and data generated from this work (IRB#: 1812394926), including all tissue and patient information acquired [44]. Informed consent was obtained from all patients by the Heart and Vascular Institute, J.W. Ruby Memorial Hospital at West Virginia University School of Medicine. Right atrial appendages were removed during open-heart and/or valvular surgeries and all tissue and data were stored in a double de-identified process. There was no incentive provided for patients. Surgeries were performed on both type 2 diabetic and non-diabetic patients, following consultation with the surgical team. Non-diabetic patients (HbA1c < 6.5 with no previous diagnosis of diabetes mellitus) and type 2 diabetic patients (HbA1c > 6.5 or with a previous diagnosis of diabetes mellitus) were designated in the study. Patients' tissue was used irrespective of sex, race, or ethnicity. Patients enrolled in the study were not part of a clinical trial. The design and execution of the study was supported by the National Heart, Lung, and Blood Institute [R01 HL-128485]. All procedures performed in studies involving human participants were in accordance with the ethical standards of the institutional and/or national research committee and with the 1964 Helsinki Declaration and its later amendments or comparable ethical standards.

Animal Model

The West Virginia University Animal Care and Use Committee approved all animal studies, including animal housing, sedation, euthanasia, and experimentation. These studies conformed to the most current National Institutes of Health (NIH) Guidelines for the Care and Use of Laboratory Animals manual. FVB/NJ (wild type) and FVB/NJ *Lepr*$^{db+/+-}$ (DbDb) male and female mice were housed in the West Virginia University Health Sciences Center Animal Facility and given access to a rodent diet and water *ad libitum*. FVB/NJ *Lepr*$^{db+/-}$ heterozygous mice were bred together to obtain a homozygous (FVB/NJ *Lepr*$^{db+/+}$) diabetic model. We have previously reported on the cardiovascular deficits of this model [6, 45, 46]. Animals in the wild-type and diabetic groups were aged to 25 weeks and were euthanized. Euthanasia was performed by sedating mice with 5% isoflurane through nose cone administration and subsequently implementing cervical dislocation. Both sexes were evaluated indiscriminately.

Consent for publication

Not applicable

Availability of Data and Materials

The datasets and computer code produced in this study are available in the following databases

- MiRNA-Seq data: Sequence Read Archive: PRJNA553501

- HITS-CLIP data: Sequence Read Archive: PRJNA553501
- LncRNA-Seq data: Sequence Read Archive: PRJNA553501
- Differential Gene Expression: Github: qahathaway/Mitochondria_PNPase_lncRNA
- Source Code: Github: qahathaway/Mitochondria_PNPase_lncRNA

Competing Interests

The authors declare that they have no competing interests

Funding

This work was supported by: The National Heart, Lung, and Blood Institute [R01 HL-128485] (JMH), American Heart Association [AHA-17PRE33660333] (QAH), American Heart Association [AHA-20PRE35080170] (AK), CoBRE Tumor Microenvironment grant support by National Institute of Health/National Institute of General Medical Sciences Grant [P20GM121322] (IM), West Virginia IDeA Network of Biomedical Research WV-INBRE support by National Institute of Health Grant [P20GM103434], WVU Genomics Core Facility support by CTSI Grant [U54GM104942], WVU Microscopy Imaging Facility for use of the Nikon A1R/N SIM-E and Dell Workstation [U54GM104942], [P20GM103434], and [P30GM103488], and the Community Foundation for the Ohio Valley Whipkey Trust.

Authors' contributions

Designing research studies (QAH, ADT, AK, MVP, MSN, JMH), conducting experiments (QAH, ADT, AK, MSN, MTW, EW, GKF, AJD, DLS), acquiring data (QAH, ADT, AK, MVP, MSN, MTW, EW), surgical procedures (CCC), analyzing data (QAH, ADT, AK, MVP, MSN), writing the manuscript (QAH, ADT, AK, MVP, MTW, EW, ARR, IM, JMH). The author Quincy A. Hathaway had full access to all the data in the study and takes responsibility for the integrity of the data and the accuracy of the data analysis. All authors read and approved the final manuscript.

Acknowledgements

We would like to acknowledge the WVU Genomics Core Facility, Morgantown WV as well as the Marshall University Genomics Core Facility, Huntington, WV for support provided to help make this publication possible. We would like to thank the West Virginia University Ruby Memorial Hospital Heart and Vascular Institute for collaborating on this work.

References

1. Wilusz JE, Sunwoo H, Spector DL: **Long noncoding RNAs: functional surprises from the RNA world**. *Genes Dev* 2009, **23**(13):1494-1504.
2. Yao RW, Wang Y, Chen LL: **Cellular functions of long noncoding RNAs**. *Nat Cell Biol* 2019, **21**(5):542-551.

3. Hathaway QA, Pinti MV, Durr AJ, Waris S, Shepherd DL, Hollander JM: **Regulating microRNA expression: at the heart of diabetes mellitus and the mitochondrion**. *Am J Physiol Heart Circ Physiol* 2018, **314**(2):H293-H310.
4. Taanman JW: **The mitochondrial genome: structure, transcription, translation and replication**. *Biochim Biophys Acta* 1999, **1410**(2):103-123.
5. Jagannathan R, Thapa D, Nichols CE, Shepherd DL, Stricker JC, Croston TL, Baseler WA, Lewis SE, Martinez I, Hollander JM: **Translational Regulation of the Mitochondrial Genome Following Redistribution of Mitochondrial MicroRNA in the Diabetic Heart**. *Circ Cardiovasc Genet* 2015, **8**(6):785-802.
6. Shepherd DL, Hathaway QA, Pinti MV, Nichols CE, Durr AJ, Sreekumar S, Hughes KM, Stine SM, Martinez I, Hollander JM: **Exploring the mitochondrial microRNA import pathway through Polynucleotide Phosphorylase (PNPase)**. *J Mol Cell Cardiol* 2017, **110**:15-25.
7. Macgregor-Das AM, Das S: **A microRNA's journey to the center of the mitochondria**. *Am J Physiol Heart Circ Physiol* 2018, **315**(2):H206-H215.
8. Zhang X, Zuo X, Yang B, Li Z, Xue Y, Zhou Y, Huang J, Zhao X, Zhou J, Yan Y *et al*: **MicroRNA directly enhances mitochondrial translation during muscle differentiation**. *Cell* 2014, **158**(3):607-619.
9. Barrey E, Saint-Auret G, Bonnamy B, Damas D, Boyer O, Gidrol X: **Pre-microRNA and mature microRNA in human mitochondria**. *PLoS One* 2011, **6**(5):e20220.
10. Gao S, Tian X, Chang H, Sun Y, Wu Z, Cheng Z, Dong P, Zhao Q, Ruan J, Bu W: **Two novel lncRNAs discovered in human mitochondrial DNA using PacBio full-length transcriptome data**. *Mitochondrion* 2018, **38**:41-47.
11. Rackham O, Shearwood AM, Mercer TR, Davies SM, Mattick JS, Filipovska A: **Long noncoding RNAs are generated from the mitochondrial genome and regulated by nuclear-encoded proteins**. *RNA* 2011, **17**(12):2085-2093.
12. Jeandard D, Smirnova A, Tarassov I, Barrey E, Smirnov A, Entelis N: **Import of Non-Coding RNAs into Human Mitochondria: A Critical Review and Emerging Approaches**. *Cells* 2019, **8**(3).
13. Zhao Y, Liu S, Zhou L, Li X, Meng Y, Li Y, Li L, Jiao B, Bai L, Yu Y *et al*: **Aberrant shuttling of long noncoding RNAs during the mitochondria-nuclear crosstalk in hepatocellular carcinoma cells**. *Am J Cancer Res* 2019, **9**(5):999-1008.
14. Bandiera S, Ruberg S, Girard M, Cagnard N, Hanein S, Chretien D, Munnich A, Lyonnet S, Henrion-Caude A: **Nuclear outsourcing of RNA interference components to human mitochondria**. *PLoS One* 2011, **6**(6):e20746.
15. Kren BT, Wong PY, Sarver A, Zhang X, Zeng Y, Steer CJ: **MicroRNAs identified in highly purified liver-derived mitochondria may play a role in apoptosis**. *RNA Biol* 2009, **6**(1):65-72.
16. Sripada L, Tomar D, Prajapati P, Singh R, Singh AK, Singh R: **Systematic analysis of small RNAs associated with human mitochondria by deep sequencing: detailed analysis of mitochondrial associated miRNA**. *PLoS One* 2012, **7**(9):e44873.

17. Dasgupta N, Peng Y, Tan Z, Ciraolo G, Wang D, Li R: **miRNAs in mtDNA-less cell mitochondria**. *Cell Death Discov* 2015, **1**:15004.
18. Shi Z, Yang WZ, Lin-Chao S, Chak KF, Yuan HS: **Crystal structure of Escherichia coli PNPase: central channel residues are involved in processive RNA degradation**. *RNA* 2008, **14**(11):2361-2371.
19. Stone CM, Butt LE, Bufton JC, Lourenco DC, Gowers DM, Pickford AR, Cox PA, Vincent HA, Callaghan AJ: **Inhibition of homologous phosphorolytic ribonucleases by citrate may represent an evolutionarily conserved communicative link between RNA degradation and central metabolism**. *Nucleic Acids Res* 2017, **45**(8):4655-4666.
20. Hui MP, Foley PL, Belasco JG: **Messenger RNA degradation in bacterial cells**. *Annu Rev Genet* 2014, **48**:537-559.
21. Zangrossi S, Briani F, Ghisotti D, Regonesi ME, Tortora P, Deho G: **Transcriptional and post-transcriptional control of polynucleotide phosphorylase during cold acclimation in Escherichia coli**. *Mol Microbiol* 2000, **36**(6):1470-1480.
22. Pobre V, Arraiano CM: **Next generation sequencing analysis reveals that the ribonucleases RNase II, RNase R and PNPase affect bacterial motility and biofilm formation in E. coli**. *BMC Genomics* 2015, **16**:72.
23. Saramago M, Barria C, Dos Santos RF, Silva IJ, Pobre V, Domingues S, Andrade JM, Viegas SC, Arraiano CM: **The role of RNases in the regulation of small RNAs**. *Curr Opin Microbiol* 2014, **18**:105-115.
24. Wang G, Chen HW, Oktay Y, Zhang J, Allen EL, Smith GM, Fan KC, Hong JS, French SW, McCaffery JM *et al*: **PNPASE regulates RNA import into mitochondria**. *Cell* 2010, **142**(3):456-467.
25. Shimada E, Ahsan FM, Nili M, Huang D, Atamdede S, TeSlaa T, Case D, Yu X, Gregory BD, Perrin BJ *et al*: **PNPase knockout results in mtDNA loss and an altered metabolic gene expression program**. *PLoS One* 2018, **13**(7):e0200925.
26. Hollander JM, Lin KM, Scott BT, Dillmann WH: **Overexpression of PHGPx and HSP60/10 protects against ischemia/reoxygenation injury**. *Free Radic Biol Med* 2003, **35**(7):742-751.
27. Li Y, Shin D, Kwon SH: **Histone deacetylase 6 plays a role as a distinct regulator of diverse cellular processes**. *FEBS J* 2013, **280**(3):775-793.
28. Lin C, Miles WO: **Beyond CLIP: advances and opportunities to measure RBP-RNA and RNA-RNA interactions**. *Nucleic Acids Res* 2019, **47**(11):5490-5501.
29. Lorenz R, Bernhart SH, Honer Zu Siederdissen C, Tafer H, Flamm C, Stadler PF, Hofacker IL: **ViennaRNA Package 2.0**. *Algorithms Mol Biol* 2011, **6**:26.
30. Gudenas BL, Wang L: **Prediction of LncRNA Subcellular Localization with Deep Learning from Sequence Features**. *Sci Rep* 2018, **8**(1):16385.
31. Han S, Liang Y, Ma Q, Xu Y, Zhang Y, Du W, Wang C, Li Y: **LncFinder: an integrated platform for long non-coding RNA identification utilizing sequence intrinsic composition, structural information and physicochemical property**. *Brief Bioinform* 2018.

32. Stothard P: **The sequence manipulation suite: JavaScript programs for analyzing and formatting protein and DNA sequences**. *Biotechniques* 2000, **28**(6):1102, 1104.
33. Calvo SE, Mootha VK: **The mitochondrial proteome and human disease**. *Annu Rev Genomics Hum Genet* 2010, **11**:25-44.
34. Long Y, Wang X, Youmans DT, Cech TR: **How do lncRNAs regulate transcription?** *Sci Adv* 2017, **3**(9):eaao2110.
35. Thomson DW, Dinger ME: **Endogenous microRNA sponges: evidence and controversy**. *Nat Rev Genet* 2016, **17**(5):272-283.
36. Paraskevopoulou MD, Vlachos IS, Karagkouni D, Georgakilas G, Kanellos I, Vergoulis T, Zagganas K, Tsanakas P, Floros E, Dalamagas T *et al*: **DIANA-LncBase v2: indexing microRNA targets on non-coding transcripts**. *Nucleic Acids Res* 2016, **44**(D1):D231-238.
37. Hayes RL, Noel JK, Mohanty U, Whitford PC, Hennelly SP, Onuchic JN, Sanbonmatsu KY: **Magnesium fluctuations modulate RNA dynamics in the SAM-I riboswitch**. *J Am Chem Soc* 2012, **134**(29):12043-12053.
38. Smith MR, Fernandes J, Go YM, Jones DP: **Redox dynamics of manganese as a mitochondrial life-death switch**. *Biochem Biophys Res Commun* 2017, **482**(3):388-398.
39. Yamanaka R, Tabata S, Shindo Y, Hotta K, Suzuki K, Soga T, Oka K: **Mitochondrial Mg(2+) homeostasis decides cellular energy metabolism and vulnerability to stress**. *Sci Rep* 2016, **6**:30027.
40. Xing YH, Chen LL: **Processing and roles of snoRNA-ended long noncoding RNAs**. *Crit Rev Biochem Mol Biol* 2018, **53**(6):596-606.
41. Khorsandi SE, Salehi S, Cortes M, Vilca-Melendez H, Menon K, Srinivasan P, Prachalias A, Jassem W, Heaton N: **An in silico argument for mitochondrial microRNA as a determinant of primary non function in liver transplantation**. *Sci Rep-Uk* 2018, **8**.
42. Bian Z, Li LM, Tang R, Hou DX, Chen X, Zhang CY, Zen K: **Identification of mouse liver mitochondria-associated miRNAs and their potential biological functions**. *Cell Res* 2010, **20**(9):1076-1078.
43. Wang G, Shimada E, Zhang J, Hong JS, Smith GM, Teitell MA, Koehler CM: **Correcting human mitochondrial mutations with targeted RNA import**. *Proc Natl Acad Sci U S A* 2012, **109**(13):4840-4845.
44. Croston TL, Thapa D, Holden AA, Tveter KJ, Lewis SE, Shepherd DL, Nichols CE, Long DM, Olfert IM, Jagannathan R *et al*: **Functional deficiencies of subsarcolemmal mitochondria in the type 2 diabetic human heart**. *Am J Physiol Heart Circ Physiol* 2014, **307**(1):H54-65.
45. Dabkowski ER, Baseler WA, Williamson CL, Powell M, Razunguzwa TT, Frisbee JC, Hollander JM: **Mitochondrial dysfunction in the type 2 diabetic heart is associated with alterations in spatially distinct mitochondrial proteomes**. *Am J Physiol Heart Circ Physiol* 2010, **299**(2):H529-540.
46. Shepherd DL, Hathaway QA, Nichols CE, Durr AJ, Pinti MV, Hughes KM, Kunovac A, Stine SM, Hollander JM: **Mitochondrial proteome disruption in the diabetic heart through targeted epigenetic regulation at the mitochondrial heat shock protein 70 (mtHsp70) nuclear locus**. *J Mol Cell Cardiol* 2018, **119**:104-115.

47. Claycomb WC, Lanson NA, Jr., Stallworth BS, Egeland DB, Delcarpio JB, Bahinski A, Izzo NJ, Jr.: **HL-1 cells: a cardiac muscle cell line that contracts and retains phenotypic characteristics of the adult cardiomyocyte**. *Proc Natl Acad Sci U S A* 1998, **95**(6):2979-2984.
48. Hathaway QA, Nichols CE, Shepherd DL, Stapleton PA, McLaughlin SL, Stricker JC, Rellick SL, Pinti MV, Abukabda AB, McBride CR *et al*: **Maternal-engineered nanomaterial exposure disrupts progeny cardiac function and bioenergetics**. *Am J Physiol Heart Circ Physiol* 2017, **312**(3):H446-H458.
49. Thapa D, Nichols CE, Lewis SE, Shepherd DL, Jagannathan R, Croston TL, Tveter KJ, Holden AA, Baseler WA, Hollander JM: **Transgenic overexpression of mitofilin attenuates diabetes mellitus-associated cardiac and mitochondria dysfunction**. *J Mol Cell Cardiol* 2015, **79**:212-223.
50. Hathaway QA, Durr AJ, Shepherd DL, Pinti MV, Brandebura AN, Nichols CE, Kunovac A, Goldsmith WT, Friend SA, Abukabda AB *et al*: **miRNA-378a as a key regulator of cardiovascular health following engineered nanomaterial inhalation exposure**. *Nanotoxicology* 2019:1-20.
51. Untergasser A, Nijveen H, Rao X, Bisseling T, Geurts R, Leunissen JA: **Primer3Plus, an enhanced web interface to Primer3**. *Nucleic Acids Res* 2007, **35**(Web Server issue):W71-74.

Figures

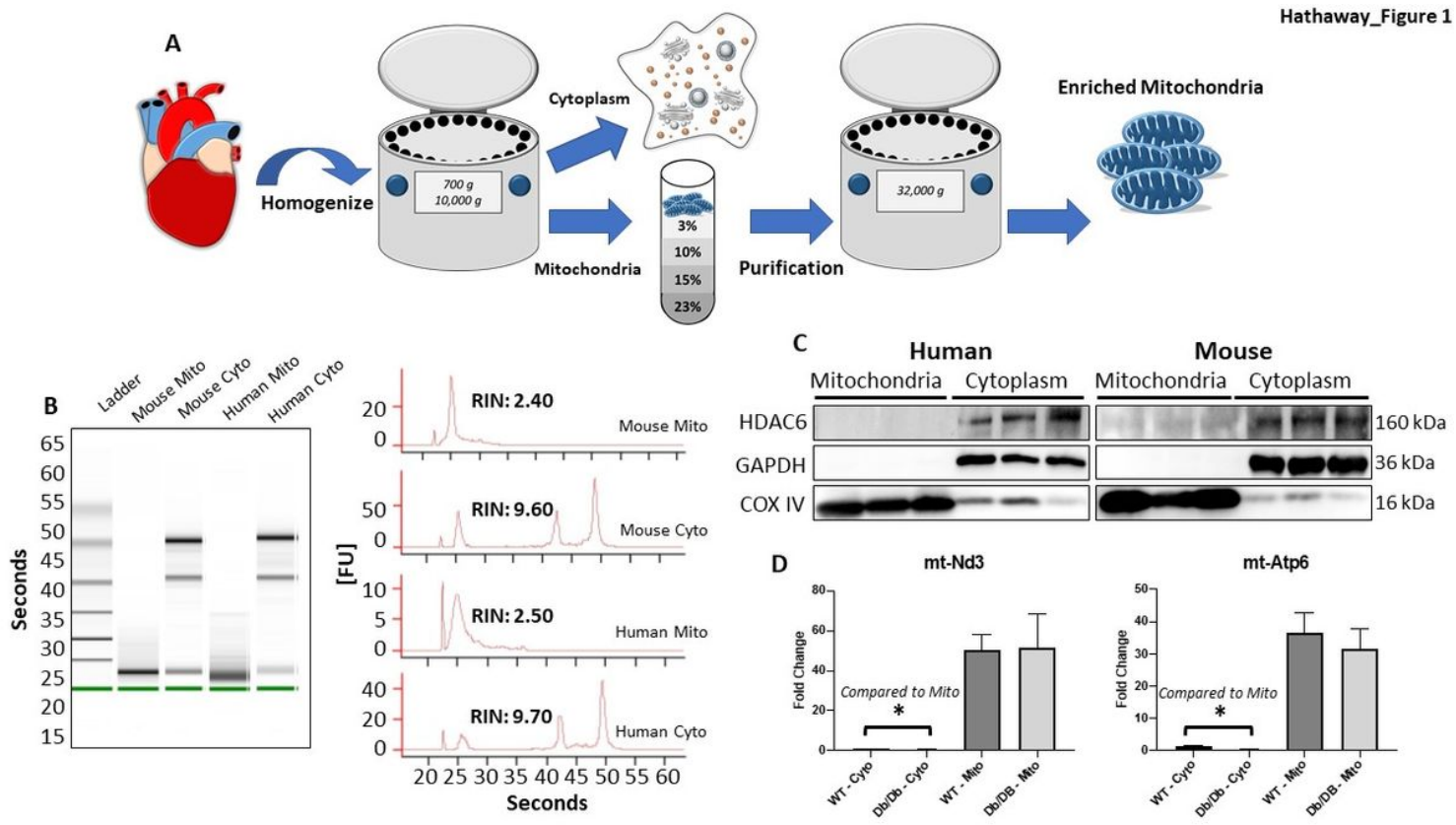

Figure 1

Enrichment of mitochondria from cardiac tissue. (A) From human atrial appendages and whole mouse hearts, samples are homogenized and differentially centrifuged to produce subcellular fractionations;

mitochondria are further sucrose-gradient purified to remove cytoplasmic contamination. (B) Purity of cytoplasmic and mitochondrial RNA is assessed through the Bioanalyzer (Agilent Technologies), with a low RNA Integrity Number (RIN) indicating limited or no presence of cytoplasmic ribosomal RNA. (C) Immunoblotting of isolated mitochondria for nuclear (HDAC6), cytoplasmic (GAPDH), and mitochondrial (COX IV) proteins in human (left) and mouse (right). (D) Real-time PCR of mitochondrial transcribed genes (mt-Nd3 and mt-Atp6) from mouse cytoplasmic and mitochondrial isolated RNA. Statistical differences are reported as the Cyto compared to Mito for both non-diabetic and diabetic cohorts. Differences between molecular and biochemical assays were considered statistically different if $P \leq 0.05$, denoted by *. A one-way analysis of variance (ANOVA) with Tukey's multiple comparisons was implemented for determining significance of qPCR. All data are presented as the mean ± standard error of the mean (SEM). mt-Nd3 = mitochondrially encoded NADH:ubiquinone oxidoreductase core subunit 3, mt-Atp6 = mitochondrially encoded ATP synthase membrane subunit 6, T2DM = type 2 diabetes mellitus, ND = non-diabetic, DbDb = FVB/NJ Leprdb_+/+ mice, WT = FVB/NJ wild-type mice, Mito = mitochondrial, Cyto = cytoplasmic, HDAC6 = histone deacetylase 6, GAPDH = glyceraldehyde 3-phosphate dehydrogenase, COX IV = cytochrome c oxidase subunit 4.

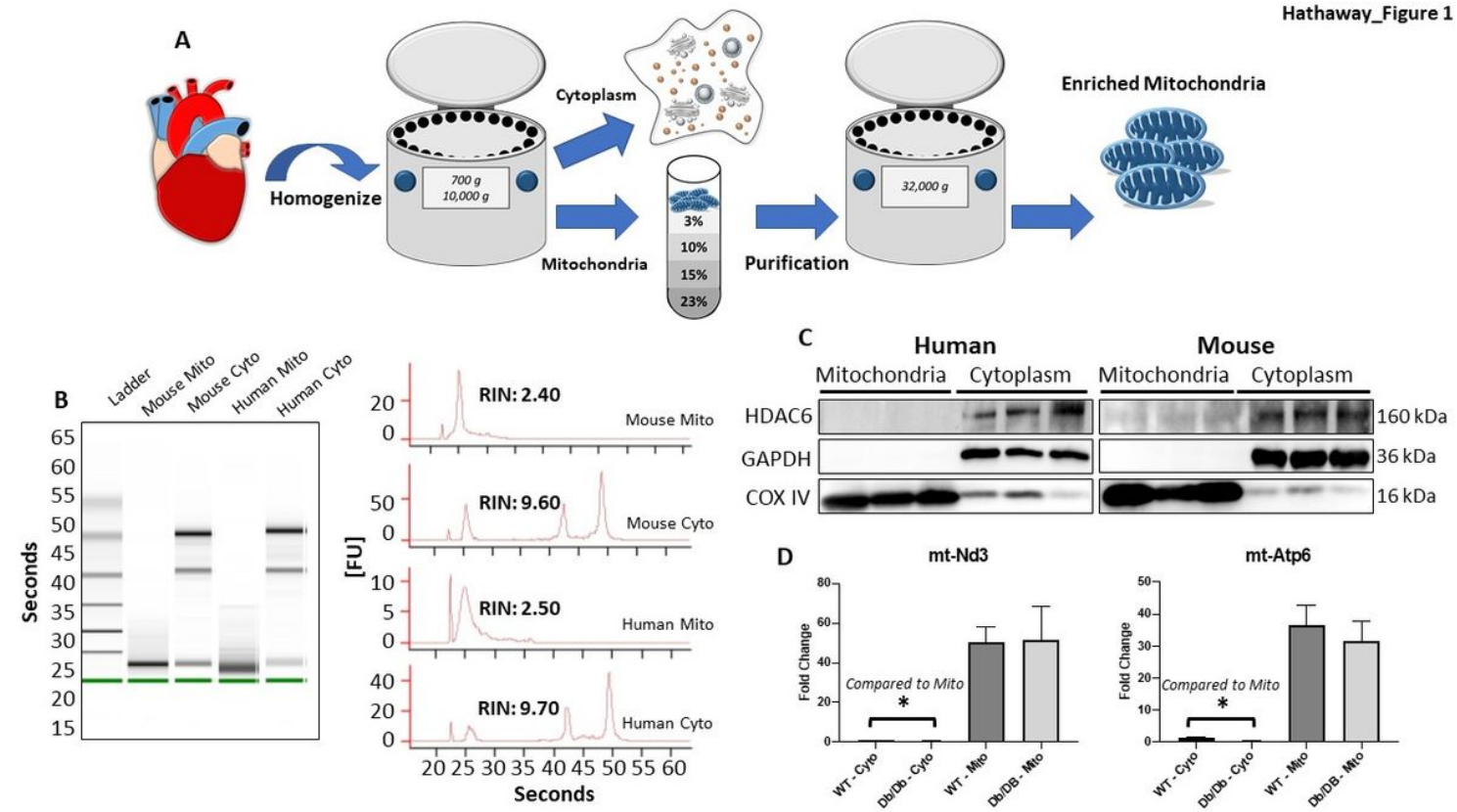

Figure 1

Enrichment of mitochondria from cardiac tissue. (A) From human atrial appendages and whole mouse hearts, samples are homogenized and differentially centrifuged to produce subcellular fractionations; mitochondria are further sucrose-gradient purified to remove cytoplasmic contamination. (B) Purity of cytoplasmic and mitochondrial RNA is assessed through the Bioanalyzer (Agilent Technologies), with a low RNA Integrity Number (RIN) indicating limited or no presence of cytoplasmic ribosomal RNA. (C)

Immunoblotting of isolated mitochondria for nuclear (HDAC6), cytoplasmic (GAPDH), and mitochondrial (COX IV) proteins in human (left) and mouse (right). (D) Real-time PCR of mitochondrial transcribed genes (mt-Nd3 and mt-Atp6) from mouse cytoplasmic and mitochondrial isolated RNA. Statistical differences are reported as the Cyto compared to Mito for both non-diabetic and diabetic cohorts. Differences between molecular and biochemical assays were considered statistically different if $P \leq 0.05$, denoted by *. A one-way analysis of variance (ANOVA) with Tukey's multiple comparisons was implemented for determining significance of qPCR. All data are presented as the mean ± standard error of the mean (SEM). mt-Nd3 = mitochondrially encoded NADH:ubiquinone oxidoreductase core subunit 3, mt-Atp6 = mitochondrially encoded ATP synthase membrane subunit 6, T2DM = type 2 diabetes mellitus, ND = non-diabetic, DbDb = FVB/NJ Leprdb_+/+ mice, WT = FVB/NJ wild-type mice, Mito = mitochondrial, Cyto = cytoplasmic, HDAC6 = histone deacetylase 6, GAPDH = glyceraldehyde 3-phosphate dehydrogenase, COX IV = cytochrome c oxidase subunit 4.

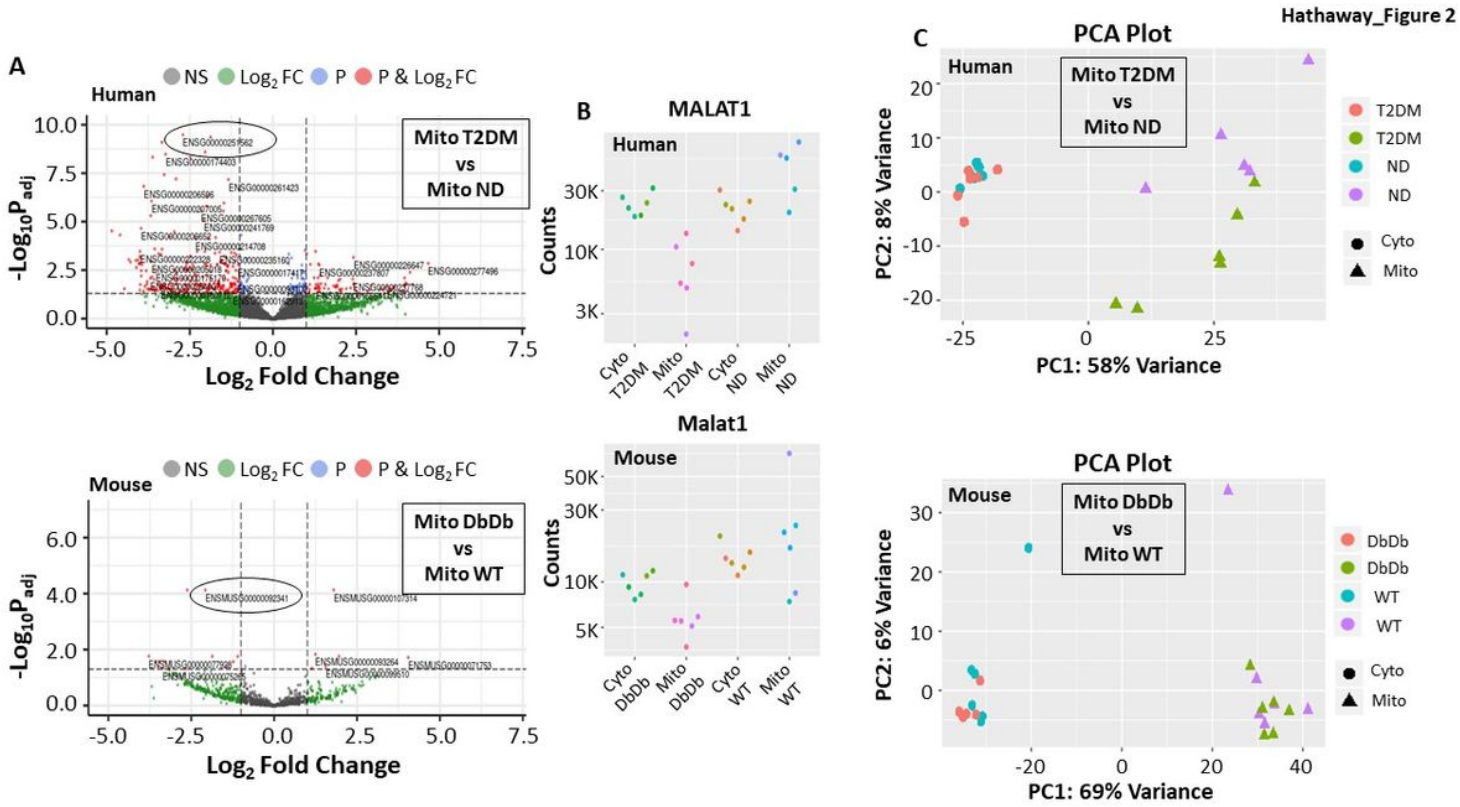

Figure 2

Characterization of long non-coding RNA (lncRNA) in the mitochondrion. Human atrial tissue (ND, n = 6: T2DM, n = 6) and mouse whole heart (WT, n = 6: DbDb, n =6) were assessed for lncRNA in the mitochondrion. (A) Volcano plots for human (top) and mouse (bottom) demonstrate the total lncRNAs differentially expressed in diabetic mitochondria, with the top gene (lowest Padj value) circled. (B) The topmost differentially regulated gene is depicted for human (top) and mouse (bottom) with the raw number of counts per each sample displayed. (C) Principle Component Analysis (PCA) for RNA in human (top) and mouse (bottom) of diabetic and non-diabetic samples for the cytoplasmic and mitochondrial portions. Values derived from sequencing are considered statistically significant when Padj < 0.05 or –

Log10Padj = 1.30. Significance was determined through the Wald test in the R environment for sequencing comparisons. Malat1 = metastasis associated lung adenocarcinoma transcript 1, T2DM = type 2 diabetes mellitus, ND = non-diabetic, DbDb = FVB/NJ Leprdb_+/+ mice, WT = FVB/NJ wild-type mice, Mito = mitochondrial, Cyto = cytoplasmic.

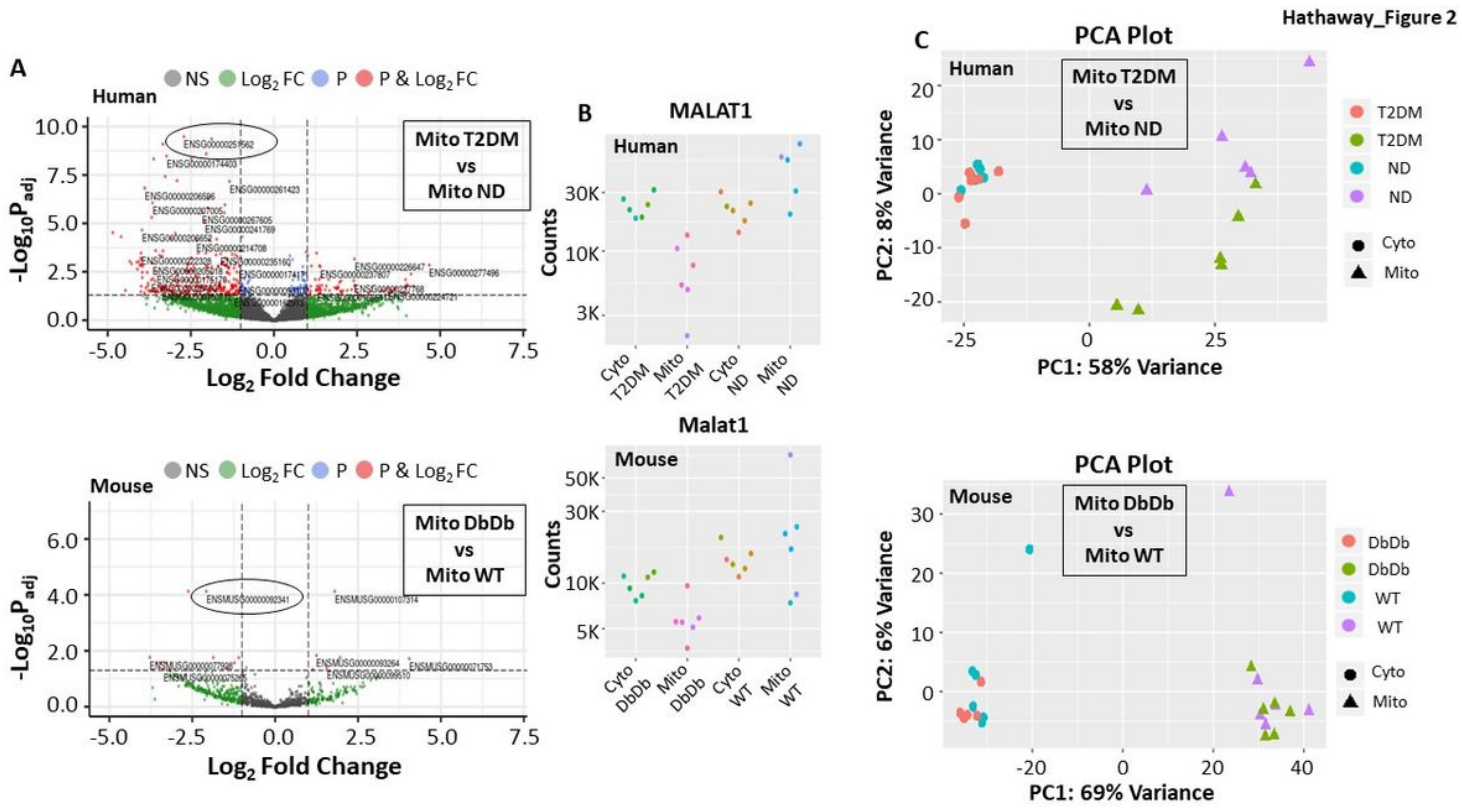

Figure 2

Characterization of long non-coding RNA (lncRNA) in the mitochondrion. Human atrial tissue (ND, n = 6: T2DM, n = 6) and mouse whole heart (WT, n = 6: DbDb, n =6) were assessed for lncRNA in the mitochondrion. (A) Volcano plots for human (top) and mouse (bottom) demonstrate the total lncRNAs differentially expressed in diabetic mitochondria, with the top gene (lowest Padj value) circled. (B) The topmost differentially regulated gene is depicted for human (top) and mouse (bottom) with the raw number of counts per each sample displayed. (C) Principle Component Analysis (PCA) for RNA in human (top) and mouse (bottom) of diabetic and non-diabetic samples for the cytoplasmic and mitochondrial portions. Values derived from sequencing are considered statistically significant when Padj < 0.05 or – Log10Padj = 1.30. Significance was determined through the Wald test in the R environment for sequencing comparisons. Malat1 = metastasis associated lung adenocarcinoma transcript 1, T2DM = type 2 diabetes mellitus, ND = non-diabetic, DbDb = FVB/NJ Leprdb_+/+ mice, WT = FVB/NJ wild-type mice, Mito = mitochondrial, Cyto = cytoplasmic.

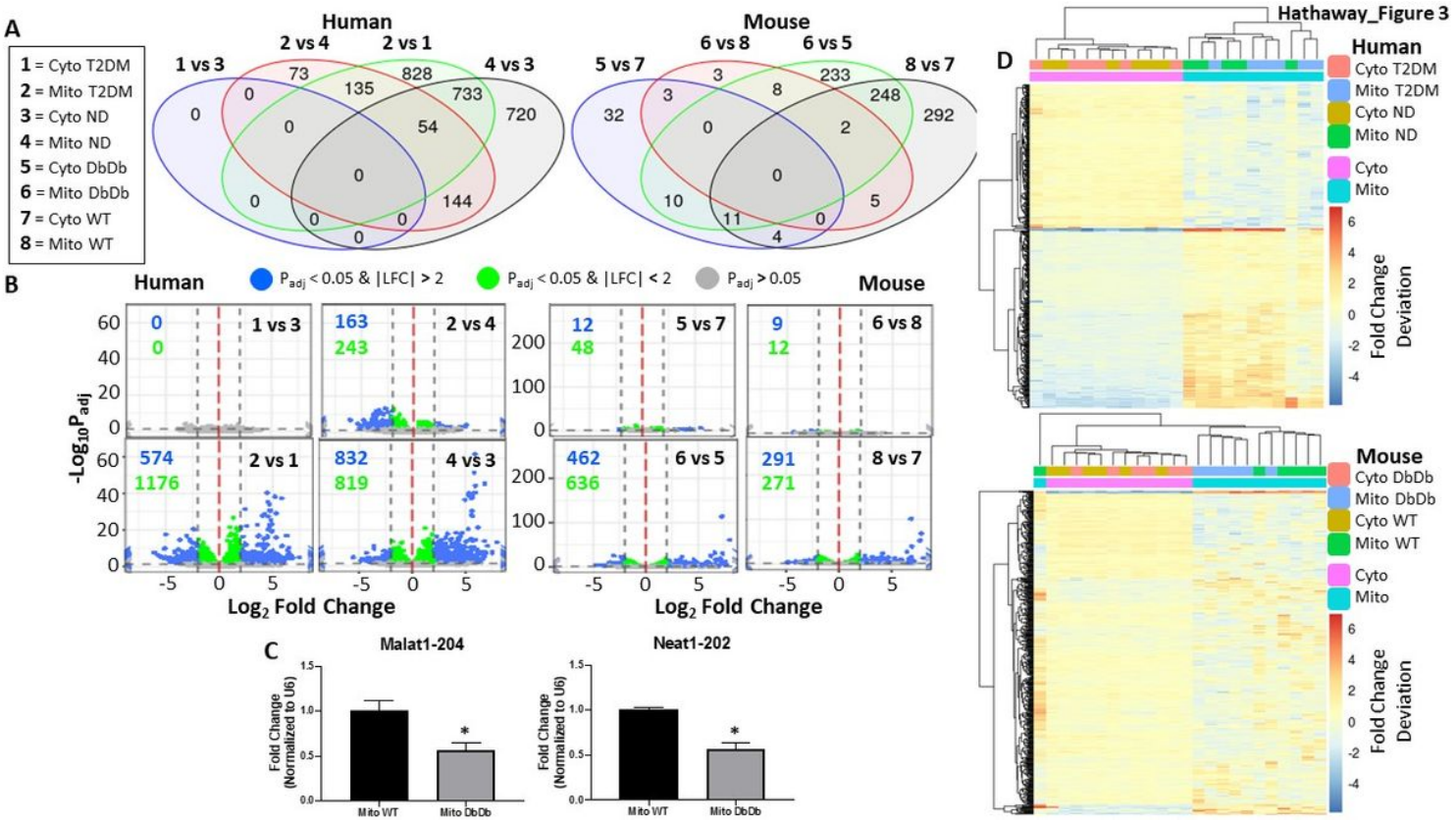

Figure 3

Expression profiles of long non-coding RNA (lncRNA) between the cytoplasm and mitochondrion. Human atrial tissue (ND, n = 6: T2DM, n = 6) and mouse whole heart (WT, n = 6: DbDb, n =6) were assessed for lncRNA in the mitochondrion. (A) Venn diagrams comparing the differential expression of genes between diabetic and non-diabetic cytoplasmic and mitochondrial fractions in human (left) and mouse (right). (B) Illustration of genes in human (left) and mouse (right) that are significantly up or downregulated between comparisons, including if the Log2 fold change is greater or less than 2. (C) QPCR to confirm the differential expression of Malat1-204 and Neat1-202 in WT (n = 4) and DbDb (n = 4) isolated mitochondria. (D) Heatmap displaying the top 500 genes with the lowest Padj value in human (top) and mouse (bottom), in both the cytoplasm and mitochondrion. Values derived from sequencing are considered statistically significant when Padj < 0.05 or –Log10Padj = 1.30. Differences between molecular and biochemical assays were considered statistically different if $P \leq 0.05$, denoted by *. Significance was determined through the Wald test in the R environment for sequencing comparisons. A two-sided Student's t-test was implemented for determining significance of qPCR. All data are presented as the mean ± standard error of the mean (SEM). LFC = Log2 Fold Change, Malat1-204 = metastasis associated lung adenocarcinoma transcript 1, transcript variant 4, Neat1-202 = nuclear paraspeckle assembly transcript 1, transcript variant 2, T2DM = type 2 diabetes mellitus, ND = non-diabetic, DbDb = FVB/NJ Leprdb_+/+ mice, WT = FVB/NJ wild-type mice, Mito = mitochondrial, Cyto = cytoplasmic.

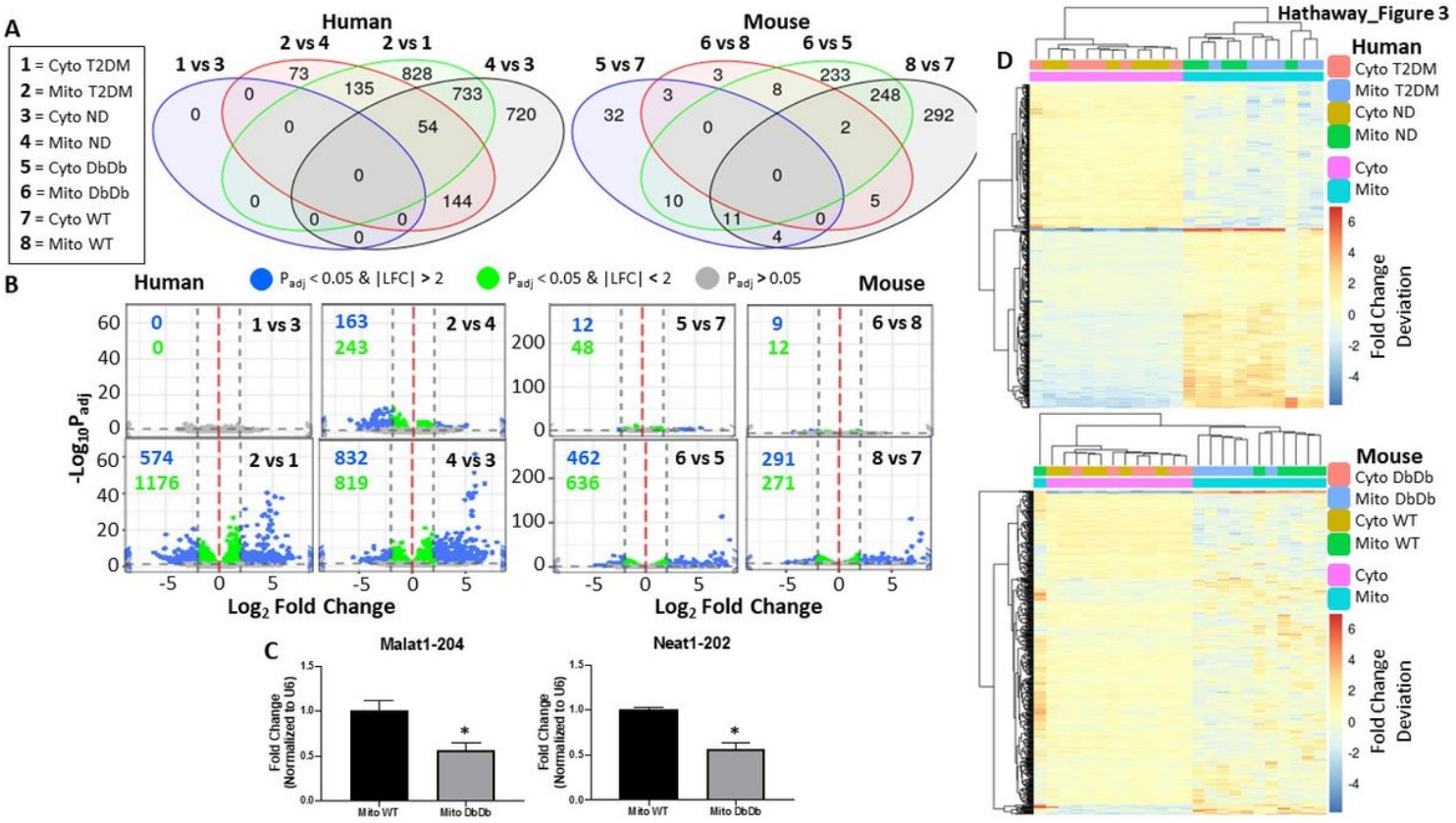

Figure 3

Expression profiles of long non-coding RNA (lncRNA) between the cytoplasm and mitochondrion. Human atrial tissue (ND, n = 6: T2DM, n = 6) and mouse whole heart (WT, n = 6: DbDb, n =6) were assessed for lncRNA in the mitochondrion. (A) Venn diagrams comparing the differential expression of genes between diabetic and non-diabetic cytoplasmic and mitochondrial fractions in human (left) and mouse (right). (B) Illustration of genes in human (left) and mouse (right) that are significantly up or downregulated between comparisons, including if the Log2 fold change is greater or less than 2. (C) QPCR to confirm the differential expression of Malat1-204 and Neat1-202 in WT (n = 4) and DbDb (n = 4) isolated mitochondria. (D) Heatmap displaying the top 500 genes with the lowest Padj value in human (top) and mouse (bottom), in both the cytoplasm and mitochondrion. Values derived from sequencing are considered statistically significant when Padj < 0.05 or –Log10Padj = 1.30. Differences between molecular and biochemical assays were considered statistically different if $P \leq 0.05$, denoted by *. Significance was determined through the Wald test in the R environment for sequencing comparisons. A two-sided Student's t-test was implemented for determining significance of qPCR. All data are presented as the mean ± standard error of the mean (SEM). LFC = Log2 Fold Change, Malat1-204 = metastasis associated lung adenocarcinoma transcript 1, transcript variant 4, Neat1-202 = nuclear paraspeckle assembly transcript 1, transcript variant 2, T2DM = type 2 diabetes mellitus, ND = non-diabetic, DbDb = FVB/NJ Leprdb_+/+ mice, WT = FVB/NJ wild-type mice, Mito = mitochondrial, Cyto = cytoplasmic.

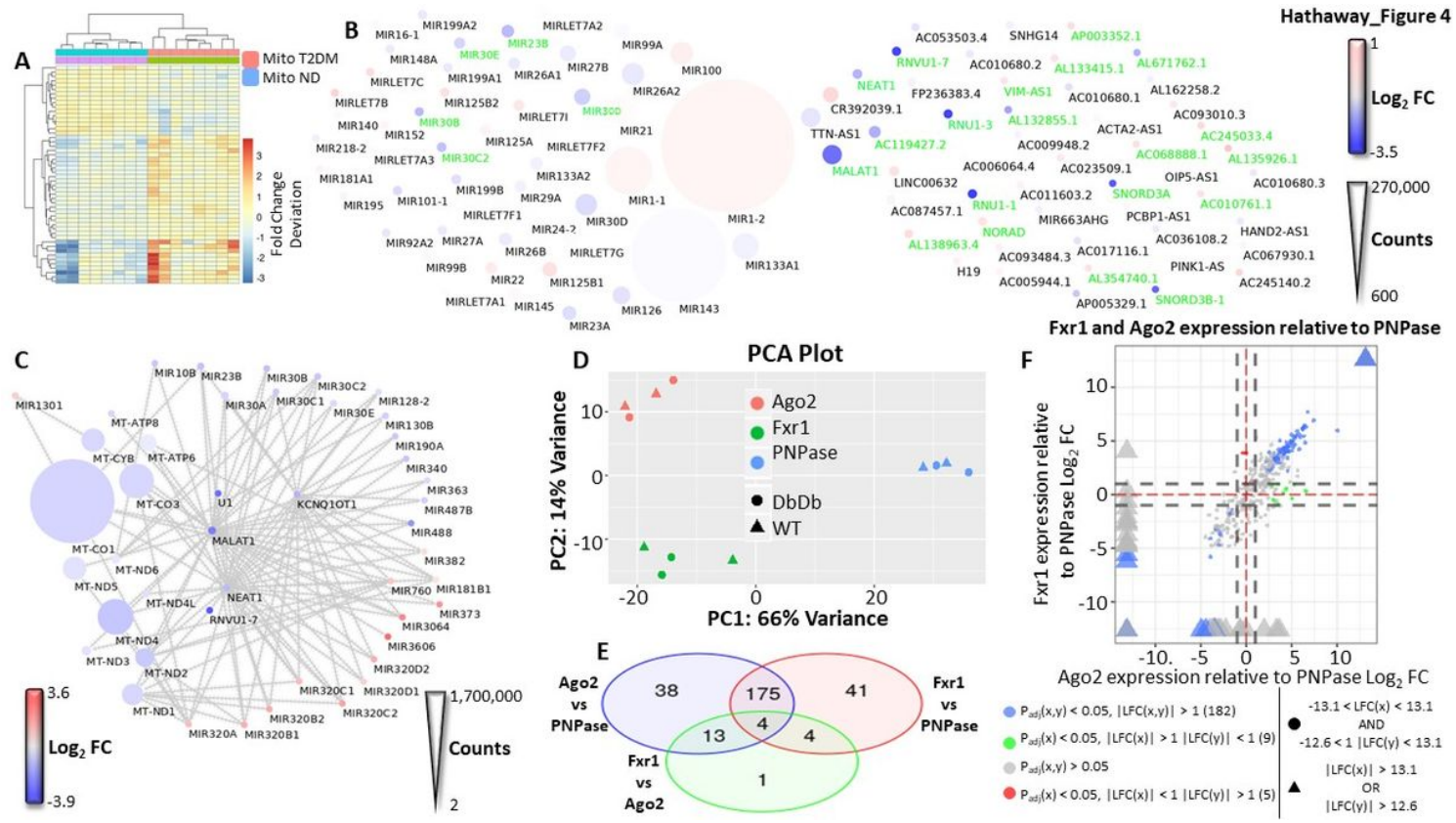

Figure 4

The interactions of long non-coding RNA (lncRNA), mRNA, and microRNA (miRNA) in mitochondria. (A) Human atrial tissue (ND, n = 8: T2DM, n = 8) were assessed for miRNA in the mitochondrion. Heatmap displaying the top 50 genes with the lowest Padj value in human mitochondria. (B) Cytoscape map depicting the 50 most abundant miRNA (left) and lncRNA (right) in human mitochondria. Size of the circle is determined by the number of counts for each gene, color of the circle is indicative of Log2 fold change of the gene, and a green label for the gene indicates that it was significantly expressed in the data set. (C) Cytoscape interaction network developed from experimentally validated RNA-RNA interactions in the NPInter (v4.0) database. Size of the circle is determined by the number of counts for each gene, color of the circle is indicative of Log2 fold change of the gene, and the directionality of the arrow indicates the affected gene. LncRNA were only included if they were differentially expressed in both human and mouse datasets. (D) Principle Component Analysis (PCA) for mouse crosslinking immunoprecipitation (CLIP) of Ago2 (n = 4), Fxr1 (n = 4), and PNPase (n = 4). (E) Venn diagrams comparing the differential expression of genes between Ago2, Fxr1, and PNPase. (F) Four Way Plot displaying the gene expression profiles of Ago2 and Fxr1 compared to PNPase. Values derived from sequencing are considered statistically significant when Padj < 0.05 or –Log10Padj = 1.30. Significance was determined through the Wald test in the R environment for sequencing comparisons. T2DM = type 2 diabetes mellitus, ND = non-diabetic, Mito = mitochondrial, Log2 FC and LFC = Log2 Fold Change, Argonaute-2 (Ago2), Fragile X mental retardation syndrome-related protein 1 (Fxr1), and Polynucleotide Phosphorylase (PNPase).

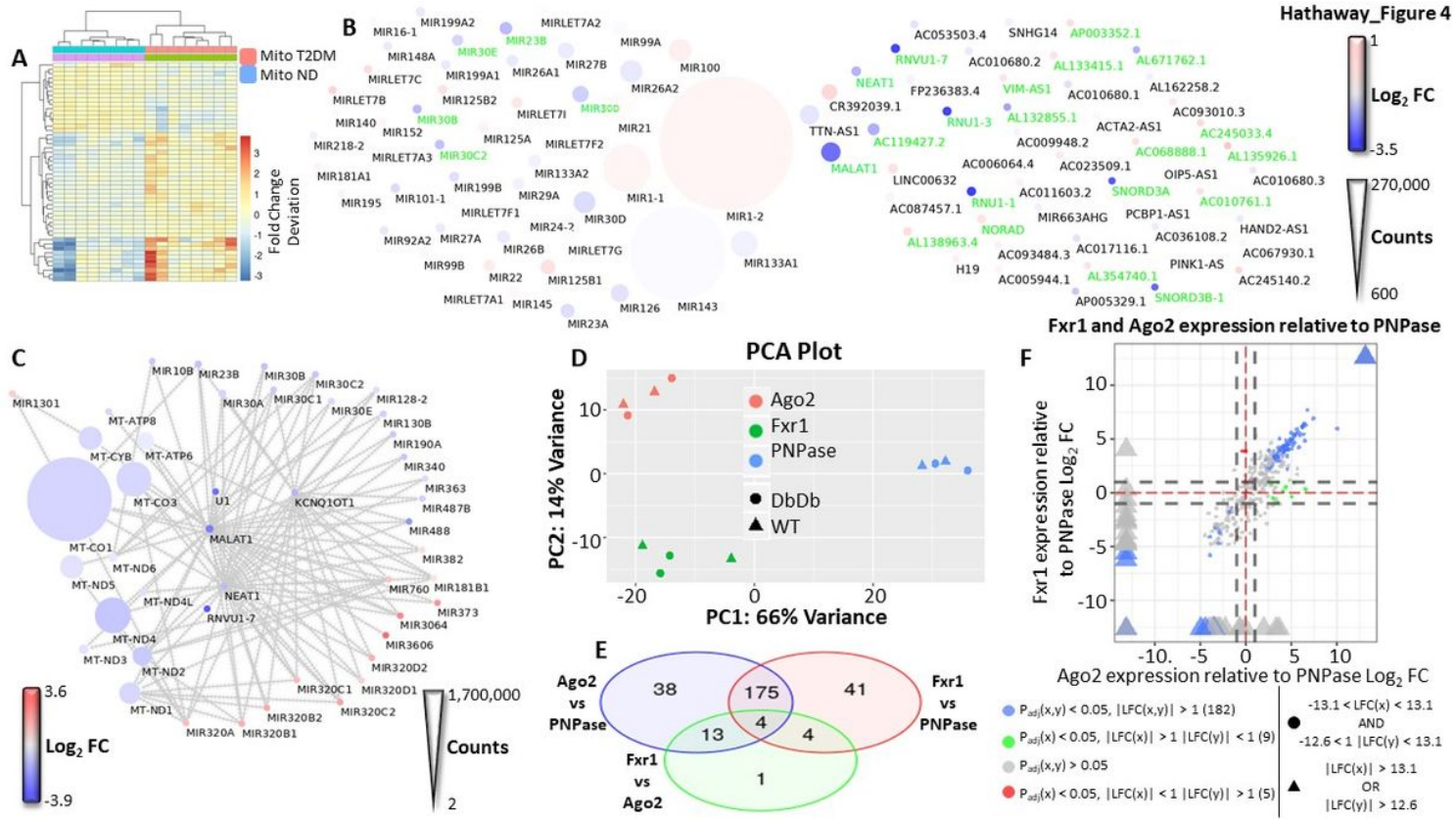

Figure 4

The interactions of long non-coding RNA (lncRNA), mRNA, and microRNA (miRNA) in mitochondria. (A) Human atrial tissue (ND, n = 8: T2DM, n = 8) were assessed for miRNA in the mitochondrion. Heatmap displaying the top 50 genes with the lowest Padj value in human mitochondria. (B) Cytoscape map depicting the 50 most abundant miRNA (left) and lncRNA (right) in human mitochondria. Size of the circle is determined by the number of counts for each gene, color of the circle is indicative of Log2 fold change of the gene, and a green label for the gene indicates that it was significantly expressed in the data set. (C) Cytoscape interaction network developed from experimentally validated RNA-RNA interactions in the NPInter (v4.0) database. Size of the circle is determined by the number of counts for each gene, color of the circle is indicative of Log2 fold change of the gene, and the directionality of the arrow indicates the affected gene. LncRNA were only included if they were differentially expressed in both human and mouse datasets. (D) Principle Component Analysis (PCA) for mouse crosslinking immunoprecipitation (CLIP) of Ago2 (n = 4), Fxr1 (n = 4), and PNPase (n = 4). (E) Venn diagrams comparing the differential expression of genes between Ago2, Fxr1, and PNPase. (F) Four Way Plot displaying the gene expression profiles of Ago2 and Fxr1 compared to PNPase. Values derived from sequencing are considered statistically significant when Padj < 0.05 or –Log10Padj = 1.30. Significance was determined through the Wald test in the R environment for sequencing comparisons. T2DM = type 2 diabetes mellitus, ND = non-diabetic, Mito = mitochondrial, Log2 FC and LFC = Log2 Fold Change, Argonaute-2 (Ago2), Fragile X mental retardation syndrome-related protein 1 (Fxr1), and Polynucleotide Phosphorylase (PNPase).

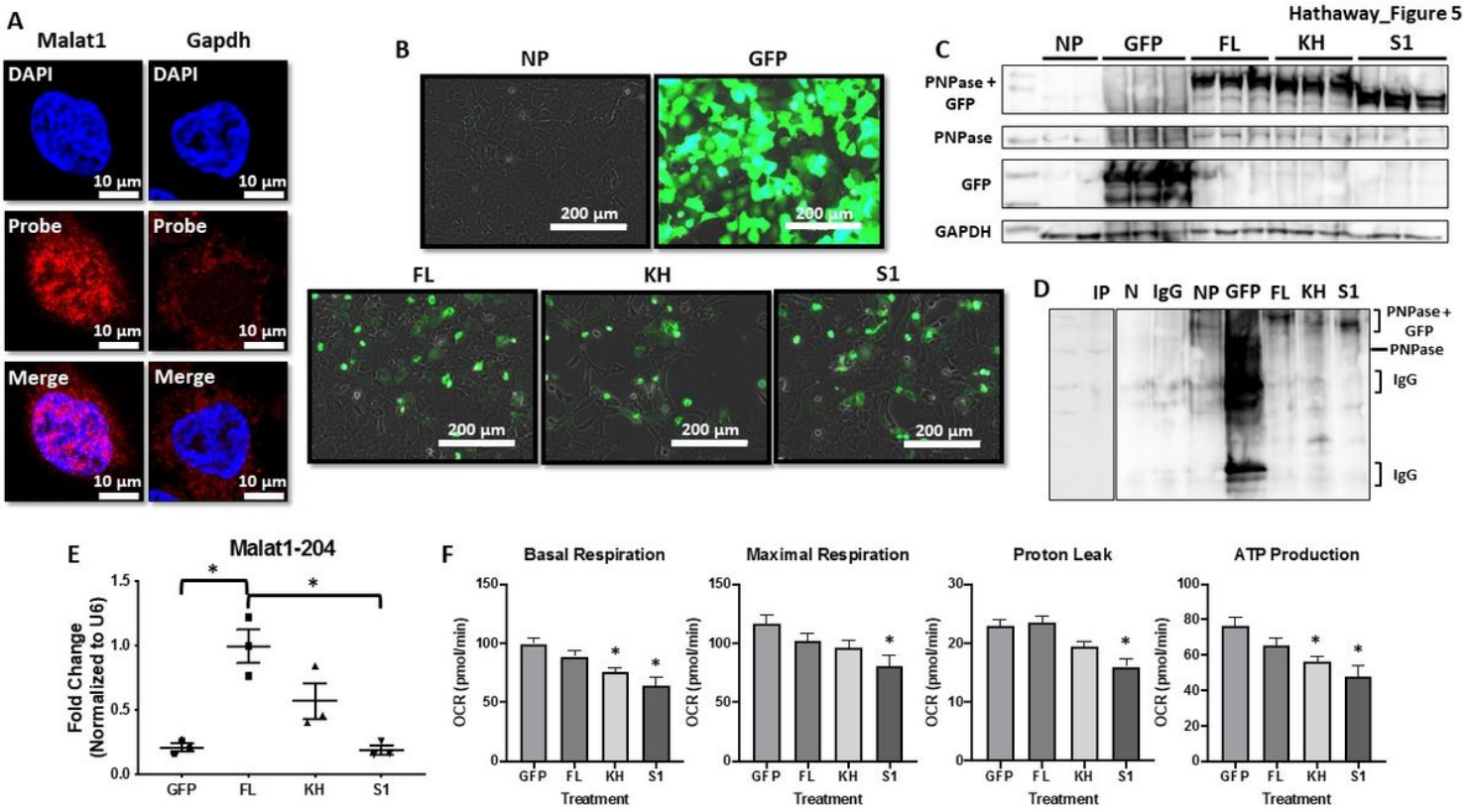

Figure 5

Malat1 compartmentalization through PNPase. (A) Confocal microscopy depicting the nucleus (DAPI, blue, emission 4 nm), probe (Malat1 or Gapdh, red, emission 570 nm), and merged image following fluorescent in situ hybridization. (B) Representative images for HL-1 cells in each group (n = 10 per group) showing fluorescence induced by pcDNA3.1+N-eGFP overexpression. (C) Immunoblotting depicting the overexpression in HL-1 cells, as well as shift in size, of the constructs. (D) A representative image of SDS-PAGE following crosslinking immunoprecipitation (CLIP) of HL-1 cells to retrieve RNA specifically bound to PNPase. (E) Real-time PCR on isolated RNA to assess binding affinity of lncRNA MALAT1 (n = 3 each group) to PNPase variants. (F) Mitochondrial respiratory capacity of HL-1 cells following transfection (n = 8 per group) with PNPase variants. Differences between molecular and biochemical assays were considered statistically different if $P \leq 0.05$, denoted by *. A one-way analysis of variance (ANOVA) with Tukey's multiple comparisons was implemented for determining significance of qPCR and mitochondrial function. All data are presented as the mean ± standard error of the mean (SEM). PNPase = polynucleotide phosphorylase, IP = input control, N = no crosslinking control, NP = no plasmid control, GFP = pcDNA3.1+N-eGFP backbone only, FL = full length PNPase open reading frame (ORF) in pcDNA3.1+N-eGFP, KH = exon 23 removed from full length PNPase in pcDNA3.1+N-eGFP, S1 = C-terminus removed from full length PNPase in in pcDNA3.1+N-eGFP, Malat1-204 = metastasis associated lung adenocarcinoma transcript 1, transcript variant 4, Malat1 = metastasis associated lung adenocarcinoma transcript 1, Gapdh = glyceraldehyde 3-phosphate dehydrogenase, OCR = oxygen consumption rate.

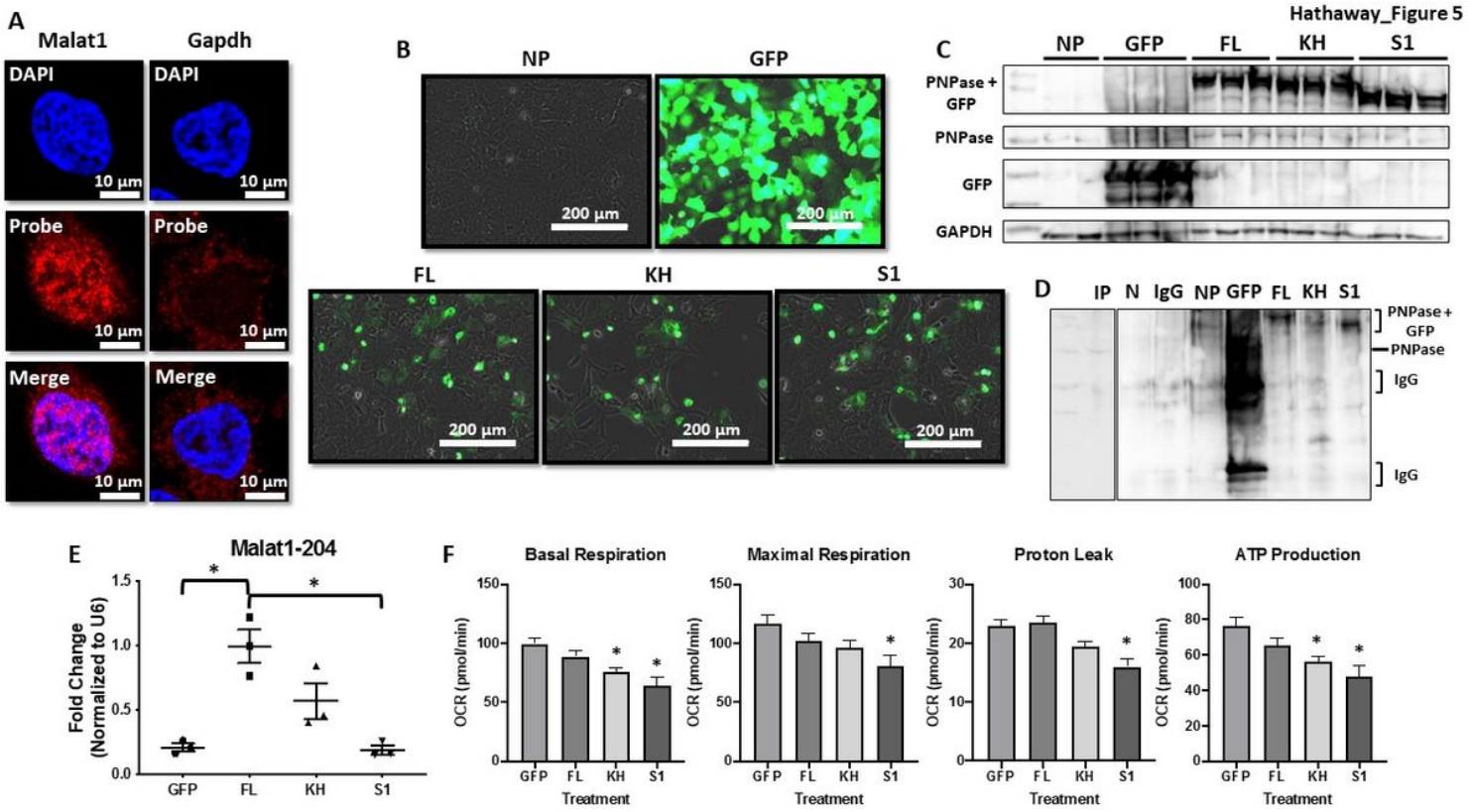

Figure 5

Malat1 compartmentalization through PNPase. (A) Confocal microscopy depicting the nucleus (DAPI, blue, emission 4 nm), probe (Malat1 or Gapdh, red, emission 570 nm), and merged image following fluorescent in situ hybridization. (B) Representative images for HL-1 cells in each group (n = 10 per group) showing fluorescence induced by pcDNA3.1+N-eGFP overexpression. (C) Immunoblotting depicting the overexpression in HL-1 cells, as well as shift in size, of the constructs. (D) A representative image of SDS-PAGE following crosslinking immunoprecipitation (CLIP) of HL-1 cells to retrieve RNA specifically bound to PNPase. (E) Real-time PCR on isolated RNA to assess binding affinity of lncRNA MALAT1 (n = 3 each group) to PNPase variants. (F) Mitochondrial respiratory capacity of HL-1 cells following transfection (n = 8 per group) with PNPase variants. Differences between molecular and biochemical assays were considered statistically different if $P \leq 0.05$, denoted by *. A one-way analysis of variance (ANOVA) with Tukey's multiple comparisons was implemented for determining significance of qPCR and mitochondrial function. All data are presented as the mean ± standard error of the mean (SEM). PNPase = polynucleotide phosphorylase, IP = input control, N = no crosslinking control, NP = no plasmid control, GFP = pcDNA3.1+N-eGFP backbone only, FL = full length PNPase open reading frame (ORF) in pcDNA3.1+N-eGFP, KH = exon 23 removed from full length PNPase in pcDNA3.1+N-eGFP, S1 = C-terminus removed from full length PNPase in in pcDNA3.1+N-eGFP, Malat1-204 = metastasis associated lung adenocarcinoma transcript 1, transcript variant 4, Malat1 = metastasis associated lung adenocarcinoma transcript 1, Gapdh = glyceraldehyde 3-phosphate dehydrogenase, OCR = oxygen consumption rate.

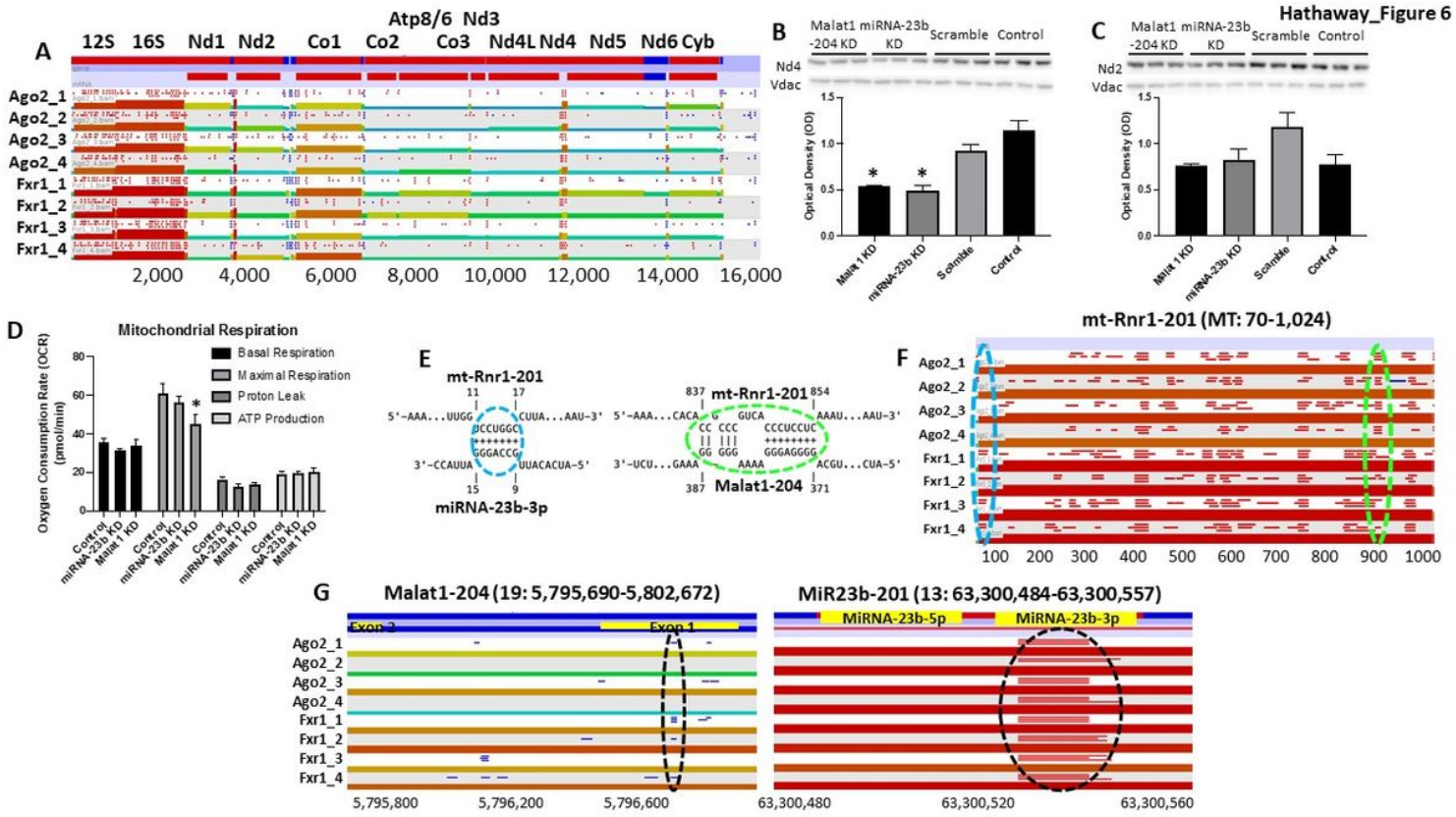

Figure 6

Malat1-204 and miRNA-23b-3p knockdown and the regulation of mitochondrial translation. (A) Mouse CLIP of Ago2 (n = 4) and Fxr1 (n = 4) displaying the reads distribution across the mitochondrial genome. Quantification between groups displays bars as thick (higher distribution of reads) and thin (lower distribution of reads). The gene regions are mapped across the top of the figure. Protein abundance of (B) mt-Nd4 and (C) mt-Nd2 were assessed in Malat1-204 and miRNA-23b-3p knockdown HL-1 cells (n = 3 per group). Malat1-204 and miRNA-23b-3p knockdown HL-1 cell lines were also assessed for (D) mitochondrial respiratory capacity (n = 10 per group). (E) Through IntaRNA 2.0, Malat-204 and miRNA-23b-3p were mapped to the mitochondrial 12S rRNA region (mt-Rnr1) to determine regions of potential binding. (F) The circled areas correlated to the predicated interactions and the CLIP data from mice showing the binding regions of Ago2 and Fxr1. (G) The complementary region of the 12S rRNA binding region (circled in black) for Malat1-204 and miRNA-23b-3p as predicted by IntaRNA 2.0. Differences between molecular and biochemical assays were considered statistically different if $P \leq 0.05$, denoted by *. A one-way analysis of variance (ANOVA) with Tukey's multiple comparisons was implemented for determining significance of immunoblotting and mitochondrial function. All data are presented as the mean ± standard error of the mean (SEM). Malat1-204 = metastasis associated lung adenocarcinoma transcript 1, transcript variant 4, OCR = oxygen consumption rate, mt-Nd2 = mitochondrially encoded NADH:ubiquinone oxidoreductase core subunit 2, mt-Nd4 = mitochondrially encoded NADH:ubiquinone oxidoreductase core subunit 4, Vdac = voltage-dependent anion channel, mt-Rnr1 = mitochondrially encoded 12S rRNA, KD = knockdown, Argonaute-2 (Ago2), Fragile X mental retardation syndrome-related protein 1 (Fxr1).

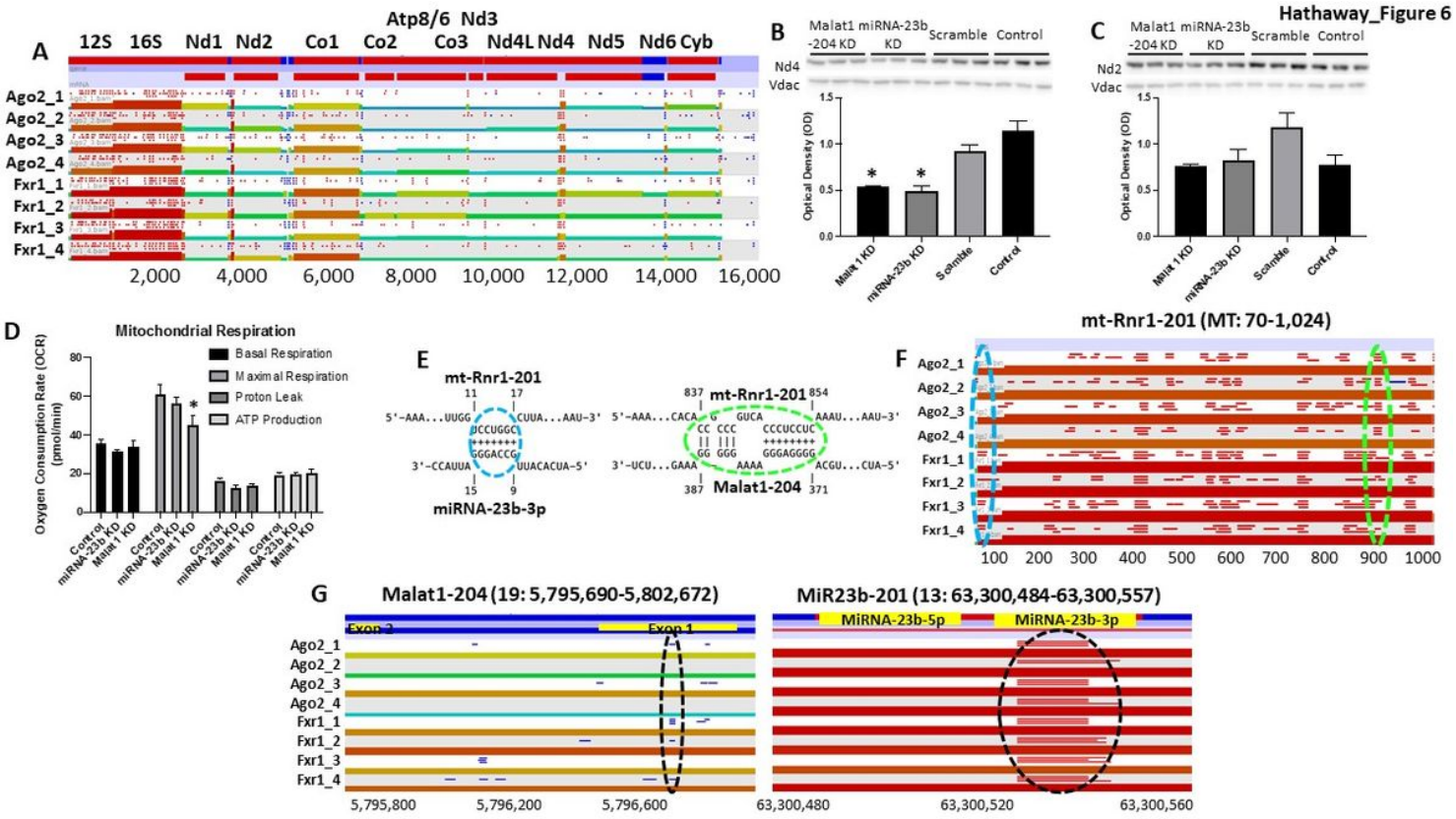

Figure 6

Malat1-204 and miRNA-23b-3p knockdown and the regulation of mitochondrial translation. (A) Mouse CLIP of Ago2 (n = 4) and Fxr1 (n = 4) displaying the reads distribution across the mitochondrial genome. Quantification between groups displays bars as thick (higher distribution of reads) and thin (lower distribution of reads). The gene regions are mapped across the top of the figure. Protein abundance of (B) mt-Nd4 and (C) mt-Nd2 were assessed in Malat1-204 and miRNA-23b-3p knockdown HL-1 cells (n = 3 per group). Malat1-204 and miRNA-23b-3p knockdown HL-1 cell lines were also assessed for (D) mitochondrial respiratory capacity (n = 10 per group). (E) Through IntaRNA 2.0, Malat-204 and miRNA-23b-3p were mapped to the mitochondrial 12S rRNA region (mt-Rnr1) to determine regions of potential binding. (F) The circled areas correlated to the predicated interactions and the CLIP data from mice showing the binding regions of Ago2 and Fxr1. (G) The complementary region of the 12S rRNA binding region (circled in black) for Malat1-204 and miRNA-23b-3p as predicted by IntaRNA 2.0. Differences between molecular and biochemical assays were considered statistically different if $P \leq 0.05$, denoted by *. A one-way analysis of variance (ANOVA) with Tukey's multiple comparisons was implemented for determining significance of immunoblotting and mitochondrial function. All data are presented as the mean ± standard error of the mean (SEM). Malat1-204 = metastasis associated lung adenocarcinoma transcript 1, transcript variant 4, OCR = oxygen consumption rate, mt-Nd2 = mitochondrially encoded NADH:ubiquinone oxidoreductase core subunit 2, mt-Nd4 = mitochondrially encoded NADH:ubiquinone oxidoreductase core subunit 4, Vdac = voltage-dependent anion channel, mt-Rnr1 = mitochondrially encoded 12S rRNA, KD = knockdown, Argonaute-2 (Ago2), Fragile X mental retardation syndrome-related protein 1 (Fxr1).

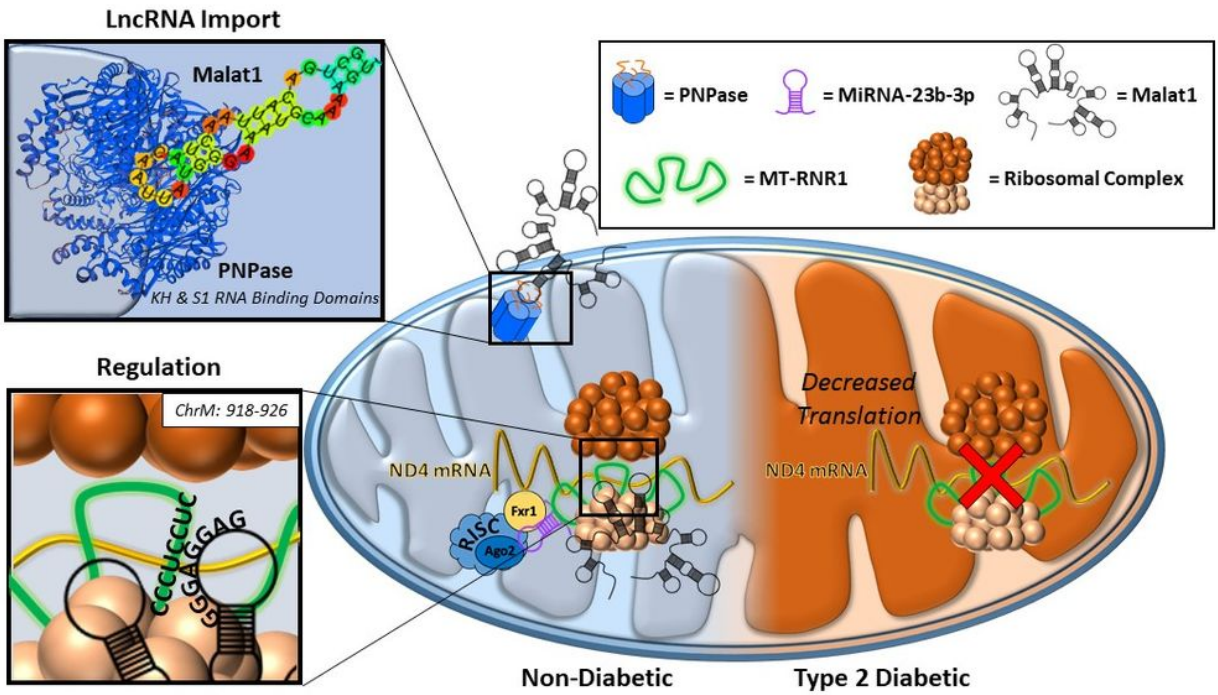

Figure 7

Illustrative overview mitochondrial regulatory network. PNPase has the capacity to bind lncRNA (Malat1) through stem-loop motifs, which may help to facilitate import of lncRNA into the mitochondrion. Within the mitochondrion, lncRNA (Malat1) could have the capacity to bind the small ribosomal subunit through 12S rRNA (mt-Rnr1) and regulate translation of mitochondrial mRNA. Ultimately, Malat1 is significantly diminished in diabetes mellitus, likely impacting the cellular response to further insult. PNPase = polynucleotide phosphorylase, Malat1 = metastasis associated lung adenocarcinoma transcript 1, mt-Nd4 = mitochondrially encoded NADH:ubiquinone oxidoreductase core subunit 4, mt-Rnr1 = mitochondrially encoded 12S rRNA.

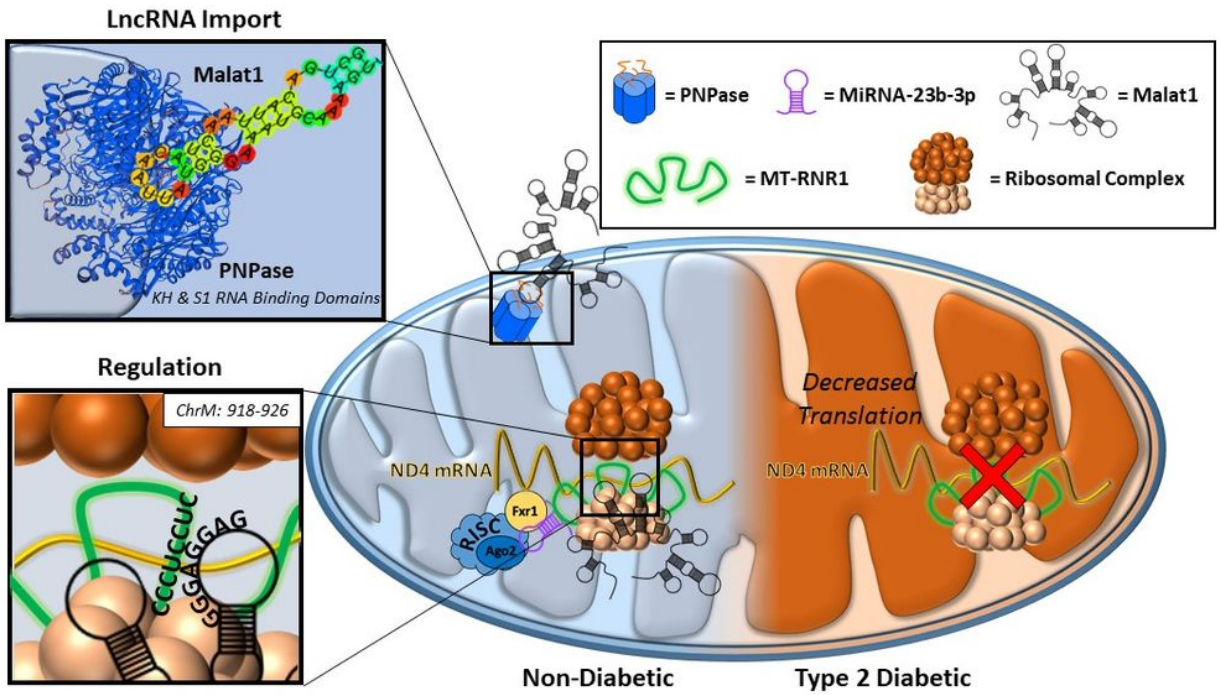

Figure 7

Illustrative overview mitochondrial regulatory network. PNPase has the capacity to bind lncRNA (Malat1) through stem-loop motifs, which may help to facilitate import of lncRNA into the mitochondrion. Within the mitochondrion, lncRNA (Malat1) could have the capacity to bind the small ribosomal subunit through 12S rRNA (mt-Rnr1) and regulate translation of mitochondrial mRNA. Ultimately, Malat1 is significantly diminished in diabetes mellitus, likely impacting the cellular response to further insult. PNPase = polynucleotide phosphorylase, Malat1 = metastasis associated lung adenocarcinoma transcript 1, mt-Nd4 = mitochondrially encoded NADH:ubiquinone oxidoreductase core subunit 4, mt-Rnr1 = mitochondrially encoded 12S rRNA.

Supplementary Files

This is a list of supplementary files associated with this preprint. Click to download.

- HathawayFigureS1.pptx
- HathawayFigureS1.pptx
- AdditionalFile1.xlsx
- AdditionalFile1.xlsx
- AdditionalFile2.docx
- AdditionalFile2.docx

- HathawayFigureS2.pptx
- HathawayFigureS2.pptx
- HathawayFigureS3.pptx
- HathawayFigureS3.pptx
- HathawayFigureS4.pptx
- HathawayFigureS4.pptx
- HathawayFigureS5.pptx
- HathawayFigureS5.pptx
- HathawayFigureS6.pptx
- HathawayFigureS6.pptx
- HathawayFigureS7.pptx
- HathawayFigureS7.pptx